



Modeling of depth-induced wave breaking under finite depth wave growth conditions

André J. van der Westhuysen¹

Received 9 April 2009; revised 28 August 2009; accepted 9 September 2009; published 26 January 2010.

[1] Recent studies have shown that the spectral wind wave model SWAN (Simulating Waves Nearshore) underestimates wave heights and periods in situations of finite depth wave growth. In this study, this inaccuracy is addressed through a rescaling of the Battjes and Janssen (1978) bore-based model for depth-induced breaking, considering both sloping bed surf zone situations and finite depth wave growth conditions. It is found that the variation of the model error with the breaker index γ_{BJ} in this formulation differs significantly between the two types of conditions. For surf zones, clear optimal values are found for the breaker index. By contrast, under finite depth wave growth conditions, model errors asymptotically decrease with increasing values of the breaker index (weaker dissipation). Under both the surf zone and finite depth wave growth conditions, optimal calibration settings of γ_{BJ} were found to correlate with the dimensionless depth $k_p d$ (where k_p is the spectral peak wave number and d is the water depth) and the local mean wave steepness. Subsequently, a new breaker index, based on the local shallow water nonlinearity, expressed in terms of the biphase of the self-interactions of the spectral peak, is proposed. Implemented in the bore-based breaker model of Thornton and Guza (1983), this breaker index accurately predicts the large difference in dissipation magnitudes found between surf zone conditions and finite depth growth situations. Hence, the proposed expression yields a significant improvement in model accuracy over the default Battjes and Janssen (1978) model for finite depth growth situations, while retaining good performance for sloping bed surf zones.

Citation: van der Westhuysen, A. J. (2010), Modeling of depth-induced wave breaking under finite depth wave growth conditions, *J. Geophys. Res.*, 115, C01008, doi:10.1029/2009JC005433.

1. Introduction

[2] The spectral wind wave model SWAN (Simulating Waves Nearshore) [Booij *et al.*, 1999] is widely used for the computation of wavefields over shelf seas, in coastal areas and in shallow lakes. The accurate estimation of wavefield statistics by such models is important to various applications in these environments. SWAN computes the evolution of wave action density N ($= E/\sigma$, where E is the variance density and σ the relative radian frequency) using the action balance equation

$$\frac{\partial N}{\partial t} + \nabla_{x,y} \cdot [(\mathbf{c}_g + \mathbf{U})N] + \frac{\partial}{\partial \theta}(c_\theta N) + \frac{\partial}{\partial \sigma}(c_\sigma N) = \frac{S_{tot}}{\sigma}, \quad (1)$$

with

$$S_{tot} = S_{in} + S_{wc} + S_{nl4} + S_{bot} + S_{brk} + S_{nl3}. \quad (2)$$

[3] The terms on the left-hand side of (1) represent, respectively, the change of wave action in time, the propa-

gation of wave action in geographical space (with \mathbf{c}_g the wave group velocity vector and \mathbf{U} the ambient current), depth- and current-induced refraction (with propagation velocity c_θ in directional space θ) and the shifting of the relative radian frequency σ due to variations in mean current and depth (with the propagation velocity c_σ). The right-hand side of (1) represents processes that generate, dissipate or redistribute wave energy, given by (2). In deep water, three source terms are used: the transfer of energy from the wind to the waves, S_{in} ; the dissipation of wave energy due to whitecapping, S_{wc} ; and the nonlinear transfer of wave energy due to quadruplet (four wave) interaction, S_{nl4} . In shallow water, dissipation due to bottom friction, S_{bot} , depth-induced breaking, S_{brk} , and nonlinear triad (three wave) interaction, S_{nl3} , are additionally accounted for.

[4] The Dutch Wadden Sea (Figure 1) is a complex coastal system that poses significant challenges to nearshore wave modeling. The region is enclosed by a series of barrier islands and the mainland coasts of the provinces of Friesland and Groningen. Tidal inlets are found between the barrier islands, each featuring an ebb tidal delta, one or more main tidal channels, and a complex system of smaller channels and flats extending into the Wadden Sea interior. Apart from the tidal channels, the Wadden Sea interior is shallow and flat, with tidally modulated depths normally ranging between 0 m (dry fall) and 3 m. During extreme storms, storm surges can cause

¹Hydraulic Engineering Unit, Deltares/Delft Hydraulics, Delft, Netherlands.

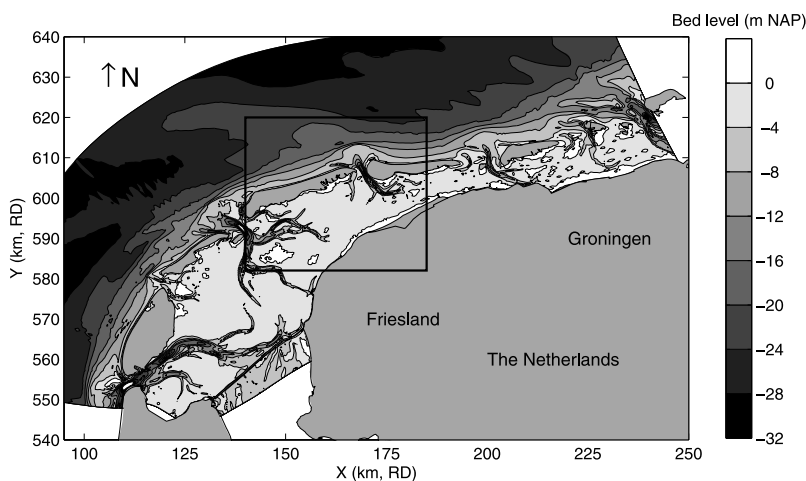


Figure 1. Bathymetry of the Dutch Wadden Sea in the north of the Netherlands, with depths in m below Normal Amsterdams Peil (NAP, Dutch leveling datum). Rectangle indicates the location of the Amelander Zeegat region (detail in Figure 2). Projection in Dutch Rijksdriehoek (RD) system.

depths over the flats to increase to up to about 6 m. The Amelander Zeegat tidal inlet (Figure 2) is found between the barrier islands of Terschelling (to the west) and Ameland (to the east). A program of wave monitoring has been operational in this inlet since 2003 [Zijderveld and Peters, 2008]. Hindcast studies based on this data [Groeneweg *et al.*, 2008; van Vledder *et al.*, 2008] have shown that the ebb tidal delta strongly shields offshore waves, so that the wavefield in the Wadden Sea interior is dominated by locally generated wind sea developing over finite depth. Moreover, it was found that SWAN typically underestimates wave heights and periods over the shallow flats. This inaccuracy can be expressed as an underestimation of the dimensionless ratio H_{m0}/d of the locally generated wind sea, where H_{m0} is the significant wave height and d the local water depth. An upper limit of H_{m0}/d of

about 0.38 appears to exist in the SWAN results, whereas observed values of as high as 0.43 are found. A number of studies for shallow Dutch lakes (Figures 3 and 4) have shown a similar tendency for SWAN to underestimate wave heights and periods under conditions of finite depth wave growth over near-horizontal topography [De Waal, 2002; Bottema and Beyer, 2002; Bottema *et al.*, 2003; van der Westhuysen *et al.*, 2007; Bottema and van Vledder, 2009]. In all these studies, a consistent underprediction of higher values of the dimensionless ratio H_{m0}/d was reported. This model inaccuracy is important to resolve, since it strongly affects the reliability of wave estimates in these finite depth environments. This issue is addressed in the present study.

[5] Under storm conditions, the locally generated waves in the Dutch Wadden Sea and shallow Dutch lakes can develop

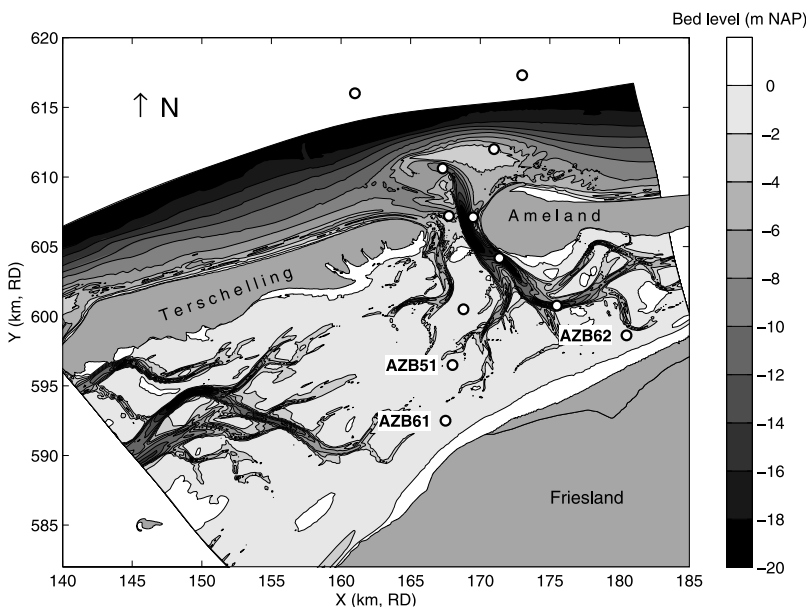


Figure 2. Bathymetry of the Amelander Zeegat region in the Dutch Wadden Sea, including the location of the wave buoys (circles). Investigated buoy locations AZB51, AZB61, and AZB62 are labeled. Depth contours in m below NAP and projection in Dutch RD system.

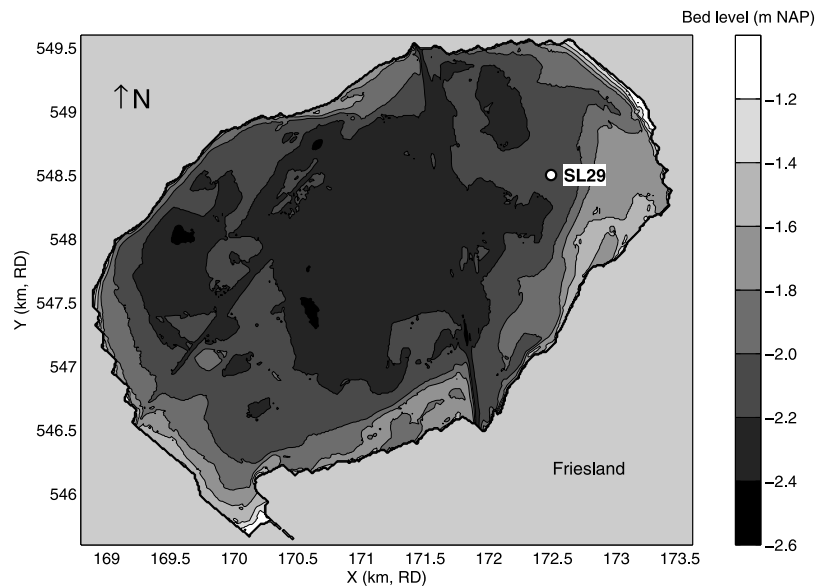


Figure 3. Bathymetry of Lake Sloten in the Netherlands, including the location of the investigated wave observation station SL29. Depth contours in m below NAP and projection in Dutch RD system.

to a finite depth wave growth limit, as described, for example, by *Bretschneider* [1958], *Young and Verhagen* [1996], and recently *Young and Babanin* [2006]. These conditions are distinct from the situation where waves are generated in deep water and subsequently dissipated due to decreasing water depth (be it a monotonically sloping, barred or terraced beach) across a surf zone toward the shore.

[6] Unlike in sloping bed surf zones, where depth-induced breaking is dominant, the above mentioned underprediction in finite depth wave growth situations may be the result of a combination of input and dissipation terms. A first possible cause of the underestimation may be underestimation of the wind input term. However, field observations in Lake George [Donelan *et al.*, 2006] suggest that the tendency of expressions such as that of *Snyder et al.* [1981] would rather be to overestimate the input, because of the omission of the process of flow separation occurring under such highly forced conditions. Analysis of source term magnitudes in SWAN shows that at greater water depths, whitecapping is the dominant dissipation term [De Waal, 2002; Bottema *et al.*, 2003; Holthuijsen *et al.*, 2008]. Over intermediate depths, bottom friction becomes important, but is surpassed in magnitude by depth-induced breaking toward smaller dimensionless depths. Accordingly, for westerly storm conditions in the Wadden Sea interior with a one year return period, whitecapping is dominant in deeper regions (2–3 m), whereas depth-induced breaking can dominate locally over the shallow banks (depths < 2 m). *Van der Westhuysen et al.* [2007] show that a reformulation of the whitecapping source term in SWAN results in an improvement in model performance over the formulation of *Komen et al.* [1984] (the default in SWAN) in finite depth wave growth situations. However, as discussed above, *Groeneweg et al.* [2008] find that despite this modification, underestimations of wave heights and periods of 12% and 10%, respectively, remain in the Wadden Sea interior. As a result, attention may be turned to the other dominant dissipation term in this region, namely depth-induced breaking.

[7] The depth-induced breaking expression of *Battjes and Janssen* [1978, hereinafter BJ78], which was developed for surf zone environments and used in SWAN, has proven to be successful in a wide range of situations. However, this formulation has mainly been studied for the case of waves from deeper water breaking on a beach. Its role in finite depth wave growth has received relatively little attention. The main

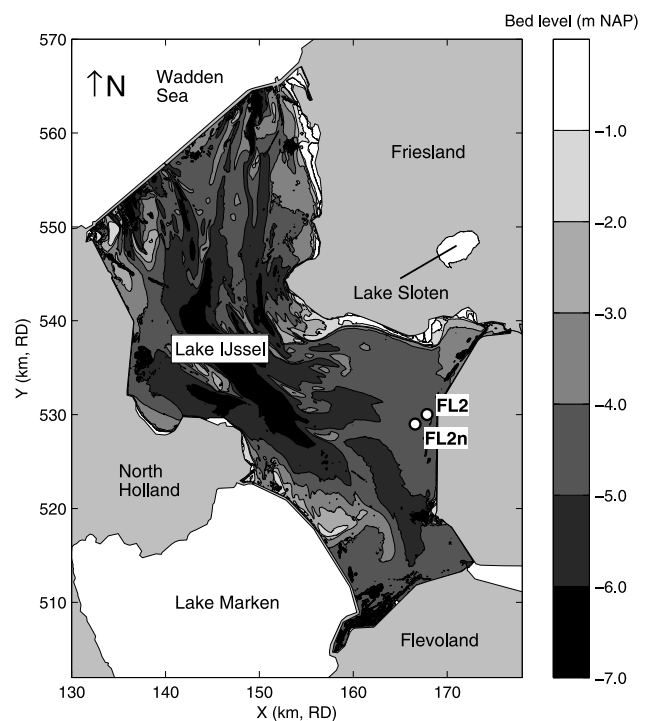


Figure 4. Bathymetry of Lake IJssel in the Netherlands, including the location of wave observation station FL2/FL2n. Depth contours in m below NAP and projection in Dutch RD system. Outline of Lake Sloten included for comparison.

calibration parameter in the formulation of BJ78 is the breaker index γ_{BJ} , originally used with a constant value of 0.8. Later studies proposed dependencies of γ_{BJ} on various wavefield variables [e.g., *Battjes and Stive*, 1985; *Nairn*, 1990; *Massel and Gourlay*, 2000; *Ruessink et al.*, 2003; *Holthuijsen and Booij*, 2006; *Aptosos et al.*, 2008].

[8] None of the expressions mentioned above explicitly take the situation of finite depth wave growth into account. Unpublished sensitivity and calibration studies for the Dutch Wadden Sea and shallow Dutch lakes (J. P. de Waal et al., unpublished study, 1997; G. P. van Vledder, unpublished study, 2003) suggest that depth-induced breaking has a significant impact on model results in these regions, and that relatively high values of approximately $\gamma_{BJ} = 0.8-0.95$ are required to correct the systematic underprediction of significant wave heights here. These results suggest that higher values of γ_{BJ} than the current default setting in SWAN (a constant $\gamma_{BJ} = 0.73$, based on the mean of the optimal values compiled by *Battjes and Stive* [1985]) would be required in situations of finite depth wave growth. However, this would imply a separate calibration setting for this class of field conditions, limiting the generality of SWAN and similar models.

[9] The aim of this study is to develop a scaling for depth-induced wave breaking that would provide improved model performance in finite depth wave growth situations, without impairing the results of the more extensively studied situation of sloping bed surf zones.

[10] To achieve the study's aims, the modeling of depth-induced breaking was studied for a data set consisting of 45 cases of laboratory and field observations, featuring, in order to ensure generality of the results, both surf zone and finite depth wave growth situations. Using this diverse data set, optimal calibration settings for γ_{BJ} were determined, and analyzed for dependencies on various parameters suggested in the literature. Based on this analysis, and the results of *Gourlay* [1994] and *Massel and Gourlay* [2000], a new estimation of the breaker index, based on the shallow water nonlinearity of the wavefield, is developed. Since this approach is not compatible with the details of the BJ78 model, the new model is based on that of *Thornton and Guza* [1983, hereinafter TG83]. The resulting nonlinearity-based model is calibrated and validated for the present data set.

[11] This paper is structured as follows: Section 2 presents the methodology followed in this study. Section 3 investigates the application of a single constant breaker index γ_{BJ} , followed by the application of a wavefield-dependent breaker index γ_{BJ} in section 4. Section 5 presents the nonlinearity-based breaker model proposed in this study. Section 6 contains a discussion of the results, and Section 7 closes the paper with conclusions.

2. Method

[12] This section presents the methodology of this study, including the models for depth-induced breaking investigated, the case selection (including a division into calibration and validation subsets) and the method used to analyze the results.

2.1. Models for Depth-Induced Breaking

[13] Two models for depth-induced breaking are investigated in this study, namely the bore-based model of BJ78,

and the adaptation of this model proposed by TG83. Both models use the analogy between the dissipation in breaking waves and a turbulent bore to describe the total rate of energy dissipation.

2.1.1. Battjes and Janssen's [1978] Model

[14] In the model of BJ78, the total dissipation due to depth-induced breaking is given by

$$D_{tot} = -\frac{1}{4} \alpha_{BJ} Q_b \bar{f} H_m^2, \quad (3)$$

in which α_{BJ} is a proportionality coefficient, Q_b represents the fraction of breakers, \bar{f} is a mean frequency (based on T_{m01} in SWAN) and H_m is maximal individual wave height. Since (2) is defined in terms of variance density, the factor ρg in the original BJ78 paper is omitted here. The maximum wave height H_m is given in BJ78 by a modified Miche expression

$$H_m = 0.88 k_p^{-1} \tanh(\gamma_{BJ} k_p d / 0.88). \quad (4)$$

[15] Expression (4) contains two limit states: for $k_p d \rightarrow \infty$ it reduces to $H_m = 0.14 L_p$, with L_p the wavelength of the peak frequency, prescribing a limit on wave steepness in deep water; for $k_p d \rightarrow 0$, it yields $H_m = \gamma_{BJ} d$, representing a depth-related limit to the wave height, determined by the breaker index γ_{BJ} . In SWAN, in which steepness breaking is modeled separately with the source term S_{wc} in (2), the former limit state is omitted to avoid double counting, so that (4) is reduced to

$$H_m = \gamma_{BJ} d. \quad (5)$$

[16] Accordingly, this relation is applied in this study. To determine the local fraction of breaking waves Q_b , BJ78 assume that the cumulative probability distribution of all wave heights is of the Rayleigh type, truncated discontinuously at $H = H_m$. This yields the following implicit expression for the fraction of breakers Q_b :

$$\frac{1 - Q_b}{-\ln Q_b} = \left(\frac{H_{rms}}{H_m} \right)^2, \quad (6)$$

in which H_{rms} is the root mean square wave height. Based on experimental results by *Battjes and Beji* [1992], the total dissipation computed by (3) is distributed over the wave spectrum proportional to the variance density, yielding the source term [*Eldeberky and Battjes*, 1996]

$$S_{brk} = D_{tot} \frac{E(\sigma, \theta)}{E_{tot}}, \quad (7)$$

where E_{tot} is the total variance.

2.1.2. Thornton and Guza's [1983] Model

[17] The model of TG83 can be regarded as a variant of the BJ78 model, with alteration primarily to the description of the wave height probability density function. In TG83 the total dissipation due to depth-induced breaking is formulated as

$$D_{tot} = -\frac{B^3 \bar{f}}{4 d} \int_0^\infty H^3 p_b(H) dH, \quad (8)$$

in which B is a proportionality coefficient and $p_b(H)$ is the fraction of waves breaking at each wave height H . Based on field observations, the wave heights in the surf zone are assumed to remain Rayleigh distributed, even after breaking. This implies that all waves will break, not only the highest, as assumed by BJ78. The probability of wave breaking $p_b(H)$ is obtained by multiplying the Rayleigh wave height probability density function $p(H)$, given by

$$p(H) = \frac{2H}{H_{rms}^2} \exp \left[-\left(\frac{H}{H_{rms}} \right)^2 \right] \quad (9)$$

by a weighting function defined so that $0 \leq W(H) \leq 1$, to yield

$$p_b(H) = W(H)p(H). \quad (10)$$

[18] Two alternatives for the weighting function are proposed by TG83. In the first, the fraction of breaking waves is independent of the wave height, and is expressed as follows:

$$W(H)_1 = \left(\frac{H_{rms}}{\gamma_{TG}d} \right)^n, \quad (11)$$

with a calibration parameter n and a breaker index γ_{TG} . Therefore, the weighting function reduces to a scaling variable that can be taken outside the integral of (8). In the second alternative, the weighting function is skewed toward larger waves, to better represent the observations

$$W(H)_2 = \left(\frac{H_{rms}}{\gamma_{TG}d} \right)^n \left\{ 1 - \exp \left[-\left(\frac{H}{\gamma_{TG}d} \right)^2 \right] \right\}. \quad (12)$$

[19] For the weighting functions (11) and (12), analytical solutions of (8) are presented in TG83. As with the BJ78 model, the source term S_{brk} in (2) can be obtained by substituting (8) into (7), under the same assumption of equal weighting of the dissipation across the spectrum as stated above.

[20] The main focus of this study is on the model of BJ78, which is used in SWAN. However, reference is made to the behavior of the TG83 model where applicable. Furthermore, the TG83 model will be used as a basis for the new breaker model developed in section 5.

2.2. Model Settings

[21] The computations presented here were performed using the SWAN model version 40.72A in stationary mode. For the deep water physics, the combination of wind input S_{in} and saturation-based whitecapping S_{wc} proposed by *van der Westhuysen et al.* [2007] was applied. Quadruplet nonlinear interaction S_{n4} was modeled using the Discrete Interaction Approximation (DIA) of *Hasselmann et al.* [1985]. The shallow water source terms include triad nonlinear interaction S_{n3} according to *Eldeberky* [1996] and bottom friction according to *Hasselmann et al.* [1973], both with their default settings in SWAN. For depth-induced breaking S_{brk} , the subject of this study, various formulations and settings were applied, as detailed in sections 3–5.

[22] The convergence criteria applied in this study are those proposed by *van der Westhuysen and van Vledder* [2008], based on the so-called curvature-based criteria of *Zijlema and van der Westhuysen* [2005].

2.3. Case Selection

[23] This investigation was conducted for a data set of field and laboratory cases which included both sloping bed surf zones and finite depth wave growth situations over near-horizontal topography. The field cases each comprise a single record in time, sampled over 1 hour unless stated otherwise. The cases considered are limited to unimodal spectra. The seven laboratory and field situations included in this data set are described below.

2.3.1. Amelander Zeegat

[24] The shallow intertidal region behind the Amelander Zeegat in the Dutch Wadden Sea (Figure 2) is the main area of application of this study. Westerly storms provide the opportunity to study finite depth wave growth over the shallow Wadden Sea interior. A selection of eleven W cases (labeled f102am07z001–011, Table 1) was made that feature high wind speeds ($U_{10} = 14–21$ m/s, being approximately uniform in time, both in speed and direction) and small water depths, yielding small values of the dimensionless depth gd/U_{10}^2 , and high values of the ratio H_{m0}/d . During these storms, twelve wave buoys, arranged in two arrays, were deployed in this region. Here only the buoys AZB51, AZB61 and AZB62 in the shallow interior are considered. Water level fields were computed with a calibrated hydrodynamic model. Spatially uniform winds were applied over the model domain, computed as the average of the wind observations at three stations in the Wadden Sea region.

2.3.2. Lake Sloten

[25] Lake Sloten in the Netherlands is approximately 4.5×3 km in size (Figure 3). It has a flat, slightly peaty bottom with a characteristic water depth of about 1.7 m. Wind and wave data for this lake have been observed at the station SL29 over the period 1999–2007 [*Bottema and van Vledder*, 2009]. Based on test cases identified by these authors, a selection of six SW cases (labeled f140slote001–006, Table 1) featuring high wind speeds ($U_{10} = 15–23$ m/s) was made, yielding small values of the dimensionless depth gd/U_{10}^2 and high values for the ratio H_{m0}/d . It should be noted that due to the limited fetch available in this small lake, the wavefield observed at station SL29 appears to not always be fully depth limited. Nonetheless, due to the small lake depth, some of the highest values of H_{m0}/d were recorded at this field site.

2.3.3. Lake IJssel

[26] Lake IJssel in the Netherlands is approximately 20×60 km in size with a typical depth of about 4–5 m, and has a fairly flat, sandy bottom (Figure 4). Wind and wave data for this lake have been observed at station FL2/FL2n over the period 1997–2007 [*Bottema and van Vledder*, 2009]. Based on test cases proposed by these authors, a selection of seven SW–W cases (labeled f130ijsse001–007, Table 1) was made that feature relatively high wind speeds ($U_{10} = 15–24$ m/s). However, due to the relatively greater water depths, larger values of the dimensionless depth gd/U_{10}^2 and smaller values of H_{m0}/d are found than for the Amelander Zeegat and Lake Sloten cases. Spatially uniform winds were applied over the model domain, computed as the spatial average of all wind

Table 1. Test Cases for Finite Depth Wave Growth^a

	Date and Time (Central European time)	U_{10} (m/s)	U_{dir} (°N)	\bar{d} (m)	$\overline{gd/U_{10}^2}$
<i>Amelander Zeegat Cases</i>					
f102am07z001	11 Jan 2007 2200	17.9	275	2.08	0.064
f102am07z002	11 Jan 2007 2240	18.8	279	2.34	0.065
f102am07z003	18 Jan 2007 1220	21.1	233	1.75	0.039
f102am07z004	18 Jan 2007 1400	20.2	263	1.55	0.037
f102am07z005	18 Jan 2007 1720	20.3	267	2.49	0.059
f102am07z006	18 Jan 2007 2040	18.9	274	3.65	0.101
f102am07z007	18 Mar 2007 1000	13.8	279	2.72	0.140
f102am07z008	18 Mar 2007 1440	18.1	266	1.86	0.056
f102am07z009	18 Mar 2007 1540	17.9	271	1.69	0.052
f102am07z010	18 Mar 2007 1700	17.1	268	1.97	0.066
f102am07z011	18 Mar 2007 1920	16.3	268	3.79	0.140
<i>Lake Sloten Cases</i>					
f140slote001	12 Feb 2002 1300	15.0	253	1.69	0.074
f140slote002	26 Feb 2002 1400	20.8	243	1.83	0.041
f140slote003	27 Oct 2002 1500	21.4	252	1.67	0.036
f140slote004	20 Mar 2004 2000	19.4	241	1.66	0.043
f140slote005	18 Jan 2007 1200	21.9	234	1.66	0.034
f140slote006	18 Jan 2007 1900	22.6	276	1.68	0.032
<i>Lake IJssel Cases</i>					
f130ijsse001	2 Oct 1999 0300	15.2	215	4.20	0.178
f130ijsse002	22 Feb 2002 0500	18.7	210	4.67	0.131
f130ijsse003	27 Oct 2002 1420	23.2	249	4.68	0.085
f130ijsse004	8 Jan 2005 1300	19.9	246	4.54	0.112
f130ijsse005	12 Feb 2005 1500	18.3	286	4.42	0.129
f130ijsse006	18 Jan 2007 1200	22.4	237	4.77	0.093
f130ijsse007	18 Jan 2007 1900	23.5	267	5.19	0.092
<i>Lake George Cases</i>					
f041lakgr001	10 Feb 1993 2200	6.4	344	1.94	0.463
f041lakgr002	3 Oct 1993 1700	10.8	342	2.14	0.180
f041lakgr003	21 Nov 1992 1600	15.2	341	2.11	0.089

^aOverbar indicates average values over all wave observation stations.

observations in the lake. No currents or water level setup were included.

2.3.4. Lake George

[27] Lake George is a shallow lake in Australia (Figure 5). When full, the lake is approximately 20 km long and 10 km wide. It has a relatively horizontal bed of fine-grained silt, with a water depth of approximately 2.5 m. The data set for Lake George considered here was recorded by *Young and Verhagen* [1996]. The selected cases (sampled over 30 minutes, labeled f041lakgr001–003, Table 1) feature a range of values for the dimensionless depth gd/U_{10}^2 and the ratio H_{m0}/d . However, due to the relatively low wind speeds for the selected cases ($U_{10} = 6–15$ m/s), these dimensionless parameters indicate the least depth limitation of the four field situations featuring finite depth wave growth (Amelander Zeegat, Lake Sloten, Lake IJssel and Lake George) considered here. Spatially varying wind fields were applied, but water levels were applied as spatially uniform.

2.3.5. DELILAH Experiment, Duck

[28] The first of the three sloping bed surf zone data sets considered is the Duck Experiment on Low-frequency and Incident-band Longshore and Across-shore Hydrodynamics (DELILAH) nearshore experiment held in October 1990 at the FRF (Field Research Facility) in Duck, North Carolina, USA, reported by *Birkemeier et al.* [1997]. The gauges of the DELILAH were located north of the FRF pier, in an area with approximately shore-parallel contours. Figure 6a shows the bed profile along the gauge array as on 6 and 15 October 1990, respectively, including the locations of the six inshore gauges considered here. Offshore boundary conditions were

recorded at 13 m depth (not shown). From the measurement data, 13 cases (sampled over 30 minutes, labeled f071delil001–013, Table 2) have been selected that feature a range of offshore wave steepnesses. The wind field and water levels are applied spatially uniformly. Ambient currents are not included.

2.3.6. Boers's [1996] Flume

[29] The second surf zone data set considered is the laboratory flume experiment by *Boers* [1996], which features a barred beach. Figure 6b shows the bed profile of this case, including the location of the wave measurement stations. All three wave conditions studied by Boers are included here, namely case 1A, featuring high steepness, case 1B, featuring high, near-breaking steepness and case 1C, featuring low steepness (labeled f031setup001–003, Table 2).

2.3.7. Battjes and Janssen's [1978] Flume

[30] The third sloping bed surf zone data set considered is the laboratory experiment of BJ78. The selected cases feature random, unidirectional waves breaking over a bar-trough beach profile. The bed profile and the observation stations are shown in Figure 6c. Two wave conditions are considered here (labeled f011wavbr001–002, Table 2). The first is Run 13 of BJ78, representing a situation with mildly breaking waves. The second is Run 15 of BJ78, representing a situation with violently breaking waves.

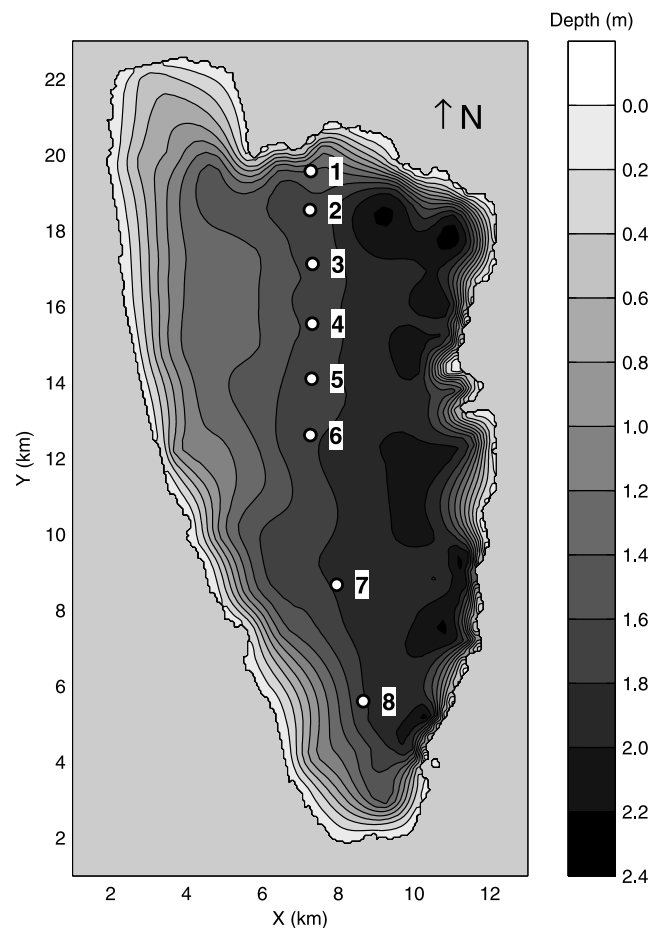


Figure 5. Bathymetry of Lake George, Australia, including the eight wave gauge stations considered.

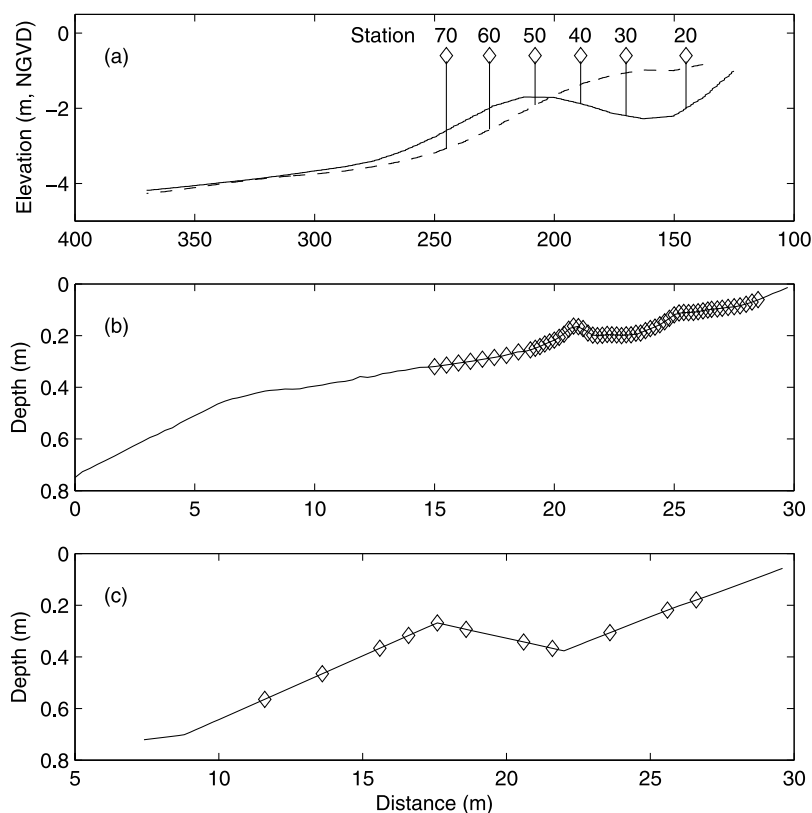


Figure 6. Bed profiles of the three sloping bed surf zone situations considered, namely, (a) the DELILAH field experiment at Duck, USA, with bed profiles as on 6 October 1990 (dashed line) and 15 October 1990 (solid line); (b) the laboratory flume experiment of *Boers* [1996]; and (c) the laboratory flume experiment of BJ78.

2.3.8. Calibration and Validation Sets

[31] The total data set of 45 laboratory and field cases was evenly divided into calibration and validation subsets (Table 3). The division was made such that the two subsets contained representative cases from both the sloping bed surf

zone cases and the finite depth wave growth cases. The relatively large data sets for the Amelander Zeegat and Duck were each equally divided into calibration and validation parts, based on values of the dimensionless depth gd/U_{10}^2 and offshore wave steepness $S_0 = H_{m,0}/L_{p,0}$, respectively. Con-

Table 2. Test Cases for Sloping Bed Surf Zones^a

	Date and Time (UTC)	$H_{m,0}$ (m)	$T_{p,0}$ (s)	U_{10} (m/s)	U_{dir} (°N)	S_0
DELILAH, Duck Cases						
	f071delil001	0.555	10.72	7.06	110	0.005
	f071delil002	0.554	9.71	1.38	236	0.006
	f071delil003	1.209	10.72	7.37	141	0.010
	f071delil004	1.120	10.72	6.92	136	0.010
	f071delil005	2.162	8.16	12.58	135	0.027
	f071delil006	1.271	8.87	4.84	129	0.014
	f071delil007	1.513	13.57	3.78	71	0.010
	f071delil008	2.546	13.57	7.44	115	0.017
	f071delil009	2.443	11.98	4.87	128	0.019
	f071delil010	2.439	11.98	3.12	142	0.019
	f071delil011	1.981	10.72	2.22	68	0.017
	f071delil012	1.648	10.72	2.72	144	0.014
	f071delil013	1.140	11.98	7.11	223	0.009
	Original Run Code	$H_{m,0}$ (m)	$T_{p,0}$ (s)	U_{10} (m/s)	U_{dir} (°N)	S_0
Boers [1996] Cases						
	1031setup001	0.157	2.05	–	–	0.033
	1031setup002	0.206	2.03	–	–	0.043
	1031setup003	0.103	3.33	–	–	0.012
BJ78 Cases						
	1011wavbr001	0.147	2.01	–	–	0.031
	1011wavbr002	0.202	1.89	–	–	0.050

^aSubscript ₀ indicates values at the model boundary. Wave steepness at model boundary computed as $S_0 = H_{m,0}/L_{p,0}$.

Table 3. Division of Calibration and Validation Subsets, Including Selection Criteria

	Selection Criteria	
	gd/U_{10}^2	S_0
<i>Calibration Cases</i>		
fl02am07z004	0.037	–
fl02am07z008	0.056	–
fl02am07z009	0.052	–
fl02am07z001	0.064	–
fl02am07z006	0.101	–
fl02am07z011	0.140	–
fl40slote001	0.074	–
fl40slote002	0.041	–
fl40slote003	0.036	–
fl40slote004	0.043	–
fl40slote005	0.034	–
fl40slote006	0.032	–
f041lakgr001	0.463	–
f041lakgr002	0.180	–
f041lakgr003	0.089	–
f071delil005	–	0.027
f071delil010	–	0.019
f071delil011	–	0.017
f071delil006	–	0.014
f071delil007	–	0.010
f071delil013	–	0.009
f071delil001	–	0.005
l031setup001	–	0.033
l031setup002	–	0.043
l031setup003	–	0.012
<i>Validation Cases</i>		
fl02am07z003	0.039	–
fl02am07z005	0.059	–
fl02am07z002	0.065	–
fl02am07z010	0.066	–
fl02am07z007	0.140	–
fl30ijsse001	0.178	–
fl30ijsse002	0.131	–
fl30ijsse003	0.085	–
fl30ijsse004	0.112	–
fl30ijsse005	0.129	–
fl30ijsse006	0.093	–
fl30ijsse007	0.092	–
f071delil009	–	0.019
f071delil008	–	0.017
f071delil012	–	0.014
f071delil003	–	0.010
f071delil004	–	0.010
f071delil002	–	0.006
l011wavbr001	–	0.031
l011wavbr002	–	0.050

sidering the relatively small number of cases contained in each of the remaining data sets (e.g., Lake Sloten, Lake George, and *Boers* [1996]), they were selected in their entirety for either the calibration or validation subsets.

2.4. Method of Analysis

[32] The analysis was performed in three steps. First, the sensitivity of the simulation results of the entire data set to variations in the breaker index γ_{BJ} in the BJ78 model, taken as spatially constant, was investigated (section 3). This analysis was repeated for γ_{TG} in the TG83 model. Secondly, based on parameterizations in the literature and correlations in the present data, it was investigated whether a variable, wavefield-dependent breaker index would yield further improvements in the simulation results (section 4). Thirdly, on the basis of the latter results, a new breaker index, based

on the local shallow water nonlinearity, is proposed and tested (section 5).

[33] The predictive ability of the investigated models for depth-induced breaking was determined on the basis of scatter index and relative bias scores, which were computed for both the significant wave height H_{m0} and the mean period $T_{m-1,0}$. These measures are defined, respectively, as

$$SCI_{\Psi} = \frac{\sqrt{\frac{1}{N} \sum_{i=1}^N (\Psi_{SWAN}^i - \Psi_{obs}^i)^2}}{\frac{1}{N} \sum_{i=1}^N \Psi_{obs}^i} \quad (13)$$

and

$$\text{Rel. bias}_{\Psi} = \frac{\sum_{i=1}^N (\Psi_{SWAN}^i - \Psi_{obs}^i)}{\sum_{i=1}^N \Psi_{obs}^i}, \quad (14)$$

where Ψ_{obs} is the observed significant wave height $H_{m0, obs}$ or mean period $T_{m-1,0, obs}$, and Ψ_{SWAN} is the corresponding modeled value $H_{m0, SWAN}$ or $T_{m-1,0, SWAN}$, in a sample of size N . These statistical measures were computed over all cases for a given laboratory or field situation (e.g., BJ78 or Amelander Zeegat). Subsequently, these individual scores were averaged to obtain overall scores for, for example, the total validation subset. A simple averaging was applied in order to give all of these data sets equal statistical weight despite the considerable difference in the number of observations contained in each set.

[34] For the calibration of the breaker models, a third statistical measure was used, namely a combined error function ε . This error function is defined in terms of the scatter indices of H_{m0} and $T_{m-1,0}$, as follows:

$$\varepsilon = \frac{1}{2} (SCI_H + SCI_T), \quad (15)$$

using the definition in (13). As above, this error function was computed over all cases for a given laboratory or field situation. By considering the mean of the error ε over a collection of cases, optimal calibration settings were determined for the total calibration subset (Table 3), as well as for its sloping bed surf zone and finite depth wave growth parts separately.

3. Constant Breaker Index γ_{BJ}

[35] First, the sensitivity of the model results for the total data set (both calibration and validation sets) to variations in the breaker index γ_{BJ} , taken as spatially constant, was considered. Figure 7 shows the variation of the scatter index SCI_H (13) and the relative bias in the significant wave height H_{m0} (14) with γ_{BJ} (range 0.30 to 1.20, taking $\alpha_{BJ} = 1$) for the individual laboratory and field data sets. In Figure 7, the results of *Boers* [1996] and BJ78 have been combined, since they show similar behavior. Clear differences can be seen between the behavior of the scatter index SCI_H and relative bias in H_{m0} for sloping bed surf zone situations on the one hand, and finite depth wave growth situations on the other. For the sloping bed surf zone situations (Figure 7 (bottom)), both the scatter index and the relative bias show a clear optimum value for γ_{BJ} , as shown, for example, by *Apotsos*

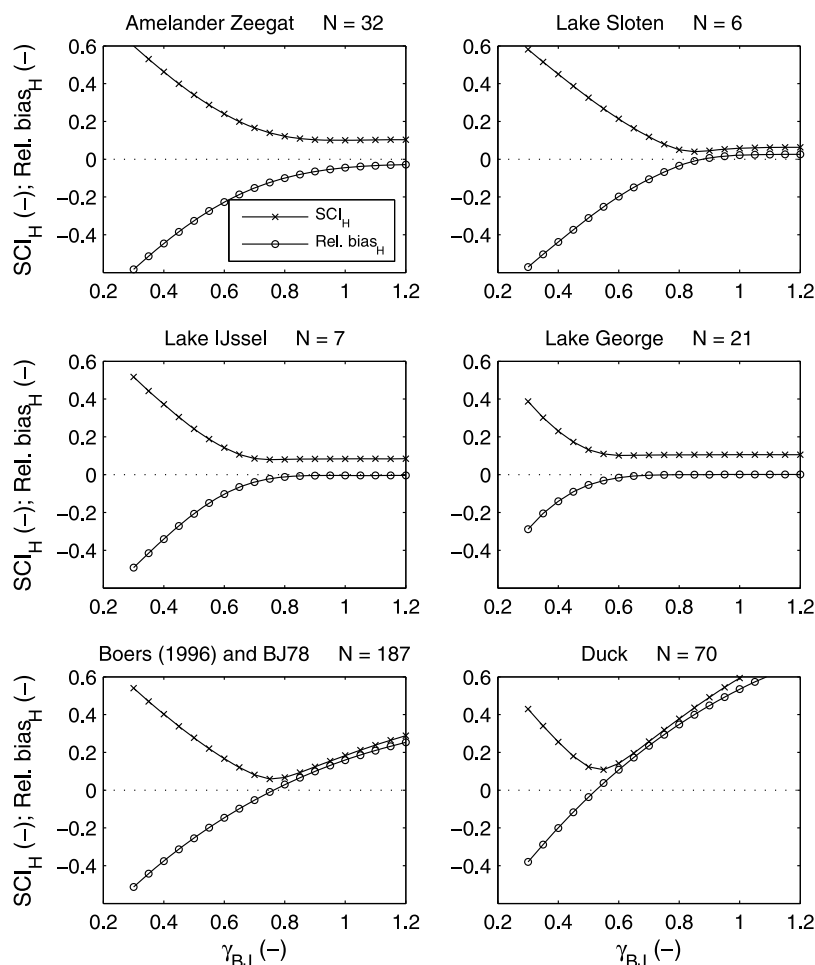


Figure 7. Variation of the scatter index SCI_H and relative bias in H_{m0} with a spatially constant γ_{BJ} in the BJ78 model, for the individual data sets. Data sets of *Boers* [1996] and BJ78 have been combined. N indicates the total number of data points included in the statistics.

et al. [2008]. This result confirms the importance of depth-induced breaking in these cases.

[36] By contrast, for the finite depth wave growth cases, the statistical error measures display an approximately asymptotic decrease in magnitude with increasing γ_{BJ} (Figure 7 (top and middle)), save for a slight positive bias at higher γ_{BJ} for Lake Sloten. At these higher values of γ_{BJ} , the BJ78 source term vanishes in strength. This behavior implies that for lower values of γ_{BJ} , including the default value in SWAN ($\gamma_{BJ} = 0.73$), the BJ78 source term produces too much dissipation in these cases. This is in agreement with earlier suggestions to this effect by *Bottema and Beyer* [2002], *Bottema et al.* [2003], and recently *Bottema and van Vledder* [2009]. This result also qualitatively agrees with field observations by *Babanin et al.* [2001] in Lake George. They found that even under strong depth limitation, depth-induced breaking accounts for only a small percentage of breaking waves under finite depth wave growth conditions (the majority of breaking events being due to excessive steepness, modeled separately by whitecapping). The present analysis explains the underestimation in H_{m0} , and hence the H_{m0}/d ratio, found in the Amelander Zeegat and Lake Sloten by *Groeneweg et al.* [2008], *De Waal* [2002], and *van der Westhuysen et al.* [2007] using the setting $\gamma_{BJ} = 0.73$.

[37] Figure 8 shows the variation of the scatter index SCI_T and the relative bias in the mean wave period $T_{m-1,0}$ with the breaker index γ_{BJ} . As with the significant wave height, the sloping bed surf zone cases show minima in the scatter index and relative bias. However, the variation of these statistical measures is much weaker than for the significant wave height (compare Figure 7). This reflects the limited influence that depth-induced breaking (as modeled here) has on the mean period $T_{m-1,0}$ in sloping bed surf zone situations. By contrast, in situations of finite depth wave growth, the setting for γ_{BJ} has a strong influence on $T_{m-1,0}$, comparable to the influence on H_{m0} . This is because under depth-limited growth conditions, the wave period actively develops along with the growing wave height. Hence, as with H_{m0} , a negative bias is generally found at the default setting for γ_{BJ} , and error statistics improve asymptotically with increasing γ_{BJ} . It should be noted that for the data sets of Lake Sloten and Lake IJssel, the asymptotically reached minimum errors in the mean period $T_{m-1,0}$ still amount to a mean bias of about -20% . This underprediction is related to the shape of the simulated spectra compared to observations, as reported earlier (with $\gamma_{BJ} = 0.73$) by *van der Westhuysen et al.* [2007] and *Bottema and van Vledder* [2009]. Finding the cause of the difference in modeled and observed spectral

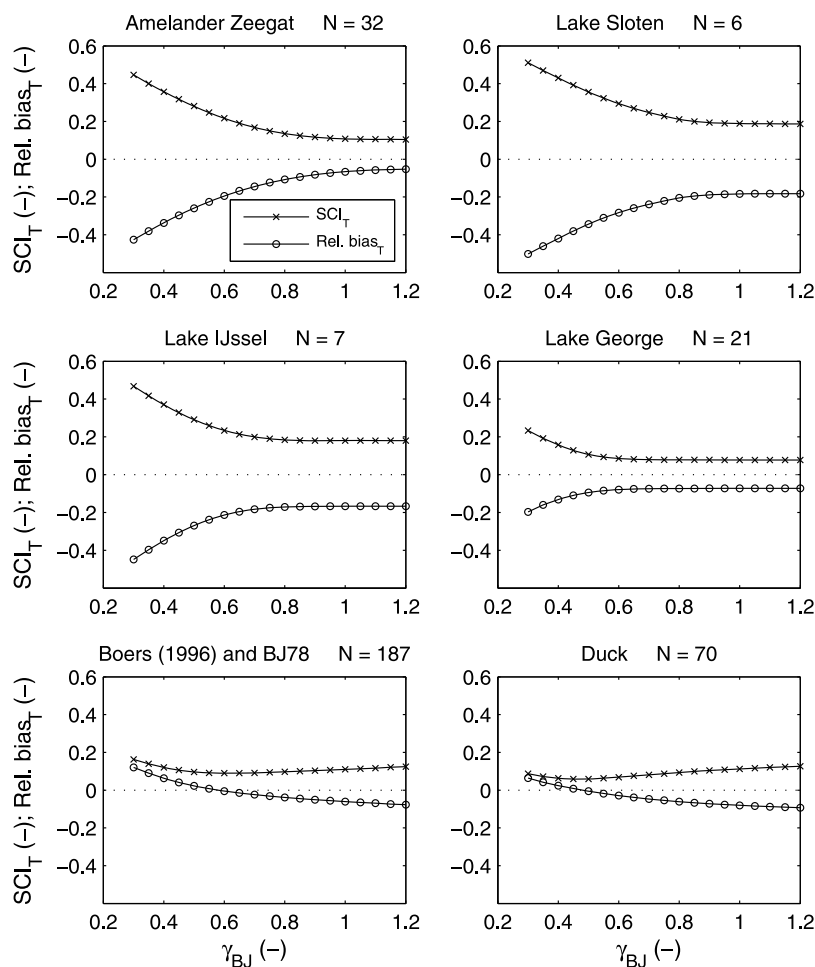


Figure 8. As in Figure 7, but now for SCI_T and relative bias in $T_{m-1,0}$.

shape is regarded as being beyond the scope of the present study.

[38] The sensitivity analysis presented above was repeated with the breaker formulation of TG83. This model displayed similar behavior to that of the BJ78 discussed here (results not shown).

[39] The results presented above suggest that no single constant value of the breaker index γ_{BJ} (or γ_{TG}) gives optimal model results under both sloping bed surf zone and finite depth wave growth situations. Hence, a variable γ_{BJ} appears necessary, optimal values of which could possibly depend on wavefield variables.

4. Wavefield-Dependent Breaker Index γ_{BJ}

4.1. Parameterizations in the Literature

[40] A number of authors have proposed parameterizations for the breaker index γ in bore-based models in terms of offshore or local wavefield characteristics. These parameterizations include dependencies of γ on the offshore wave steepness [Battjes and Stive, 1985; Nairn, 1990], the local dimensionless depth $k_p d$ [Ruessink et al., 2003], a dissipation rate based on a normalized surf zone width [Holthuijsen and Booij, 2006] and the offshore wave height and the inverse Iribarren number [Apotsos et al., 2008]. Here it is investi-

gated whether any of these proposed dependencies of γ_{BJ} could explain the model behavior observed in section 3, and provide a parameterization for γ_{BJ} suitable for both surf zone and finite depth wave growth situations.

[41] The analysis was done by setting out the optimal value of γ_{BJ} for each data point in the complete data set (calibration plus validation) against a range of local parameters found at that point. The optimal value of γ_{BJ} was determined on the basis of the results of the sensitivity analysis performed in section 3. For each combination of field or laboratory case and observation location, the spatially constant setting of γ_{BJ} yielding the smallest SCI_T at that data point was identified as its optimum γ_{BJ} value. This approach was followed instead of the inverse modeling technique applied by Ruessink et al. [2003], due to the low spatial density of observation points in the finite depth wave growth cases. Although the approach applied here neglects the spatial coherence between neighboring data points, it proved sufficient to identify trends in the variation of γ_{BJ} among the various laboratory and field situations. In this analysis only the least squares error in H_{m0} is considered in order to facilitate comparison with previous studies in the literature. Since the cases featuring finite depth wave growth were found to typically show an asymptotic decrease in prediction error with increasing γ_{BJ} , the optimal value of γ_{BJ} was taken as the lowest value of this

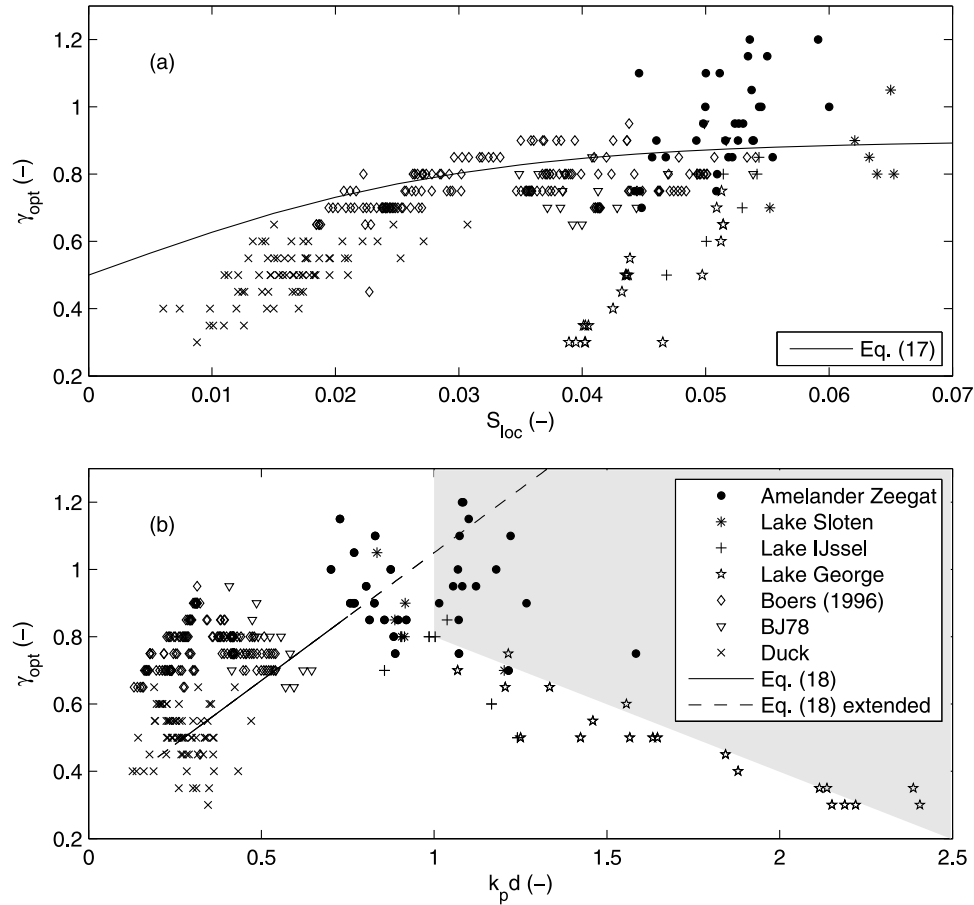


Figure 9. Scatterplots of optimal values of γ_{BJ} (based on minimum SCI_H) versus (a) local wave steepness and (b) local dimensionless depth $k_p d$. Included in Figure 9a is the parameterization (17) of *Vink* [2001], based on *Battjes and Stive* [1985]. Figure 9b includes the parameterization (18) of *Ruessink et al.* [2003], with solid line indicating the original range of $k_p d$ and dashed line the extension based on the present data.

parameter for which the error in H_{m0} is within 0.5% of the overall minimum error in H_{m0} (which was typically at the highest value of γ_{BJ} investigated).

[42] A number of dependencies of the breaker index γ on wavefield characteristics proposed in the literature do not apply to the situation of finite depth wave growth in isolated water bodies. Offshore variables such as the offshore wave steepness [Battjes and Stive, 1985; Nairn, 1990] and offshore wave height and inverse Iribarren number based on the offshore steepness [Apotsos et al., 2008] are not defined for such situations, and can therefore not be used directly. However, *Vink* [2001] proposes to apply the parameterization of *Battjes and Stive* [1985], with the offshore wave steepness replaced by a local wave steepness

$$S_{loc} = \frac{H_{rms} k_{mn}}{2\pi}, \quad \text{with} \quad k_{mn} = \left[\frac{\iint k^{-\frac{1}{2}} E(\sigma, \theta) d\sigma d\theta}{E_{tot}} \right]^{-2}, \quad (16)$$

in which H_{rms} and k_{mn} are the local root mean square wave height and a mean wave number, respectively. This is the first parameterization considered.

4.2. Dependency on Local Wave Steepness

[43] Figure 9a shows the variation of the optimal value of γ_{BJ} (on the basis of minimum SCI_H) with S_{loc} for the complete data set. It can first be seen that the cases featuring finite depth wave growth generally have higher values for the local steepness S_{loc} than those featuring sloping bed surf zones. A weak correlation between the local steepness and the optimal values of γ_{BJ} can be seen: the lower steepnesses of the sloping bed surf zone cases correspond to generally lower optimal values of γ_{BJ} , whereas the higher values of S_{loc} found for the Amelander Zeegat and Lake Sloten correspond to higher optimal values for γ_{BJ} . However, Lake George and some data points of Lake IJssel show a different trend, namely low optimal values of γ_{BJ} at relatively high wave steepness. This behavior, related to the greater dimensionless depth found in these cases, is discussed below.

[44] Also included in Figure 9a is the parameterization of γ_{BJ} proposed by *Vink* [2001], based on *Battjes and Stive* [1985]

$$\gamma_{BJ} = 0.5 + 0.4 \tanh(33S_{loc}), \quad (17)$$

where the local wave steepness S_{loc} is given by (16). This parameterization captures the general trend of the data, but does not adequately follow the data of either the sloping bed cases (particularly Duck) or the finite depth growth cases (particularly the Amelander Zeegat). Nor does it describe the Lake George data, and the mentioned Lake IJssel data, well. It can be concluded that wave steepness alone does not fully characterize the conditions, and hence is not able to fully specify the required setting of γ_{BJ} .

4.3. Dependency on Local $k_p d$ Value

[45] Another distinguishing feature of waves generated over finite depth is that they have relatively high values of the dimensionless depth kd compared to sloping bed surf zone situations. *Ruessink et al.* [2003] found, for the breaker model of *Baldock et al.* [1998] (equivalent to BJ78 for the milder slopes considered here), a correlation between the optimum value of γ_{BJ} and the product of a local characteristic wave number (using the peak wave number k_p , D. J. R. Walstra, personal communication, 2008) and the water depth d , for a collection of sloping bed surf zone cases. They propose the following linear relationship between these variables:

$$\gamma_{BJ} = 0.76k_p d + 0.29. \quad (18)$$

[46] Figure 9b shows the correlation between the optimal values of γ_{BJ} (again based on the minimum SCI_H) and the local $k_p d$ for the total data set, featuring both sloping bed surf zones and finite depth growth cases. Also included in Figure 9b is the parameterization (18). The relationship between $k_p d$ and the optimal values for γ_{BJ} can be seen to form two well-defined groups. First, for values of approximately $k_p d < 1$, including the cases of Duck, BJ78, *Boers* [1996], and most data points of the Amelander Zeegat, Lake Sloten and Lake IJssel, a positive correlation between optimal γ_{BJ} values and $k_p d$ appears to exist. Most of this data agrees with (18) extended to beyond the $k_p d = 0.7$ upper limit considered by *Ruessink et al.* [2003]. The exception is the data of *Boers* [1996], which have somewhat higher optimal γ_{BJ} values than given by (18). For the second group of data, for values of approximately $k_p d > 1$, the optimal γ_{BJ} values display a negative correlation with $k_p d$. This occurs for the same cases found to break the general trend of (17) above, namely, the cases of Lake George and some of Lake IJssel. Some cases of the Amelander Zeegat and Lake Sloten can also be seen to belong to this group. This negative trend with $k_p d$ occurs because at increasing dimensionless depth the influence of depth-induced breaking steadily decreases. Therefore, only progressively smaller values of γ_{BJ} (yielding greater dissipation) still produce an underestimation of H_{m0} . Hence, the value for γ_{BJ} at which the SCI_H reaches an asymptotic minimum (the value plotted in Figure 9b) progressively reduces. Because of the asymptotic decrease in error with increasing γ_{BJ} in this $k_p d$ region, all γ_{BJ} values higher than the plotted ones (shaded region) would give a minimum SCI_H . Hence, in an operational setting, these data points would also be adequately modeled using (18). Represented in terms of $k_p d$, these cases can be distinguished from the shallower water data of the former group, which, save for the data of *Boers* [1996], follow (18).

[47] Considering the agreement between (18), proposed by *Ruessink et al.* [2003], and our data set featuring both sloping bed and finite depth wave growth cases, the parameterization (18) was applied in simulations with the validation subset. This was done without further calibration. Figure 10 compares the scatterplot results of model and observations, obtained with the BJ78 model using the default setting $\gamma_{BJ} = 0.73$ and using the parameterization (18), respectively. It can be seen that (18), when applied to the validation subset, yields a significant improvement in model results over the constant γ_{BJ} . Most significantly, for the finite depth cases of the Amelander Zeegat, the systematic underprediction of H_{m0} (Figure 10 (top)) and higher values of H_{m0}/d (Figure 10 (bottom)) reported by *Groeneweg et al.* [2008] is removed. For the cases of Duck, the overprediction of H_{m0} and H_{m0}/d found with $\gamma_{BJ} = 0.73$ is largely corrected by the application of (18). These improvements are the direct result of the higher and lower values of γ_{BJ} , respectively, prescribed by (18) relative to the constant $\gamma_{BJ} = 0.73$. For the sloping bed cases, these results can be considered to agree with those of *Ruessink et al.* [2003]. A general improvement in the predicted mean period $T_{m-1,0}$ can also be seen. Consequently, the overall statistical scores improve significantly relative to those found with the default setting for γ_{BJ} .

[48] It can be concluded that the general agreement of our data set with (17) (using local steepness) and (18) suggests that for both sloping bed surf zones and finite depth growth cases, depth-induced breaking is not solely determined by the ratio H_m/d given in (5), but also (at least) by wave steepness and the dimensionless depth $k_p d$. *Battjes and Stive* [1985] and *Ruessink et al.* [2003] derived (17) (using offshore steepness) and (18), respectively, by means of inverse modeling, but neither study provided a physical explanation for the proposed relationships. The dependencies of γ_{BJ} on the local wave steepness and the dimensionless depth $k_p d$ suggest links with the shallow water nonlinearity. The possibility of basing the breaker index on this wavefield characteristic is explored next.

5. Breaker Index Based on Wavefield Nonlinearity

5.1. Model Description

[49] Expressions for depth-induced breaking in phase-averaged wave models have traditionally featured a basic dependency on the ratio of wave height to water depth. However, some authors have suggested the use of shallow water nonlinearity in the context of wave breaking. *Nelson* [1985, 1994] applies a shallow water nonlinearity parameter $F_c = g^{1.25} H^{0.5} T^{2.5} / d^{1.75}$, proposed by *Swart and Laubser* [1978] and closely related to the Ursell number, in an analysis of maximum stable wave heights on a coral reef top. Using laboratory data of regular waves, *Gourlay* [1994] argues that F_c , when based on the deep water wave height in front of a reef H_0 and the water depth at the reef edge d_e , is a suitable parameter for classifying wave transformation and dissipation levels over a reef front. For wave prediction purposes over reef fronts, *Massel and Gourlay* [2000] apply this definition of F_c to scale the breaking intensity of the BJ78 bore model in its periodic form. This indicates support for applying shallow water nonlinearity to the problem of depth-induced breaking, as also suggested by the analysis in

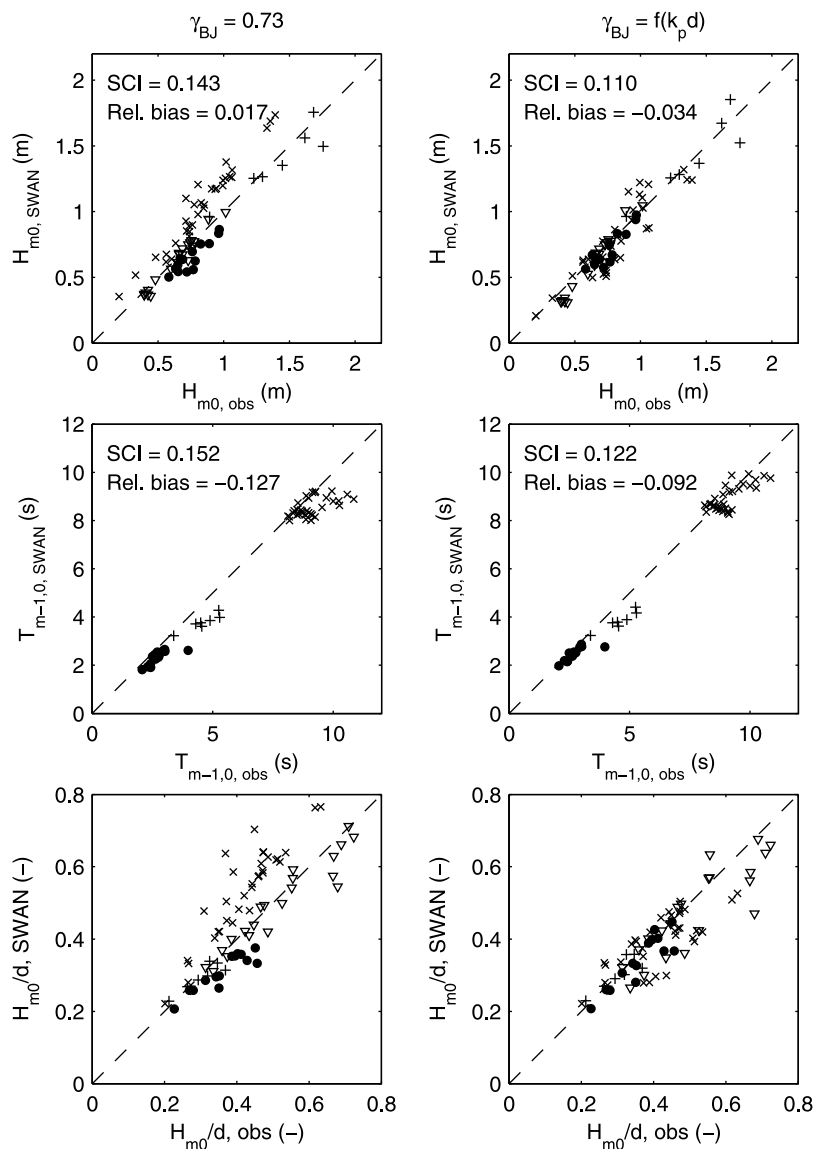


Figure 10. Scatterplots of model results versus observations of the validation subset for the BJ78 model (left) with the default setting of γ_{BJ} and (right) as parameterized with (18) proposed by *Ruessink et al.* [2003]. Plotted are results of Amelander Zeegat (solid circles), Lake IJssel (pluses), Duck (crosses), and the BJ78 flume (inverted triangles). Wave height data of BJ78 are scaled up by a factor of 5 for presentation purposes.

section 4. However, the parameterization of *Massel and Gourlay* [2000] is applicable only to reef fronts. In particular, due to its definition in terms of offshore wave height H_0 , it is unsuitable for application to finite depth wave growth in isolated water bodies such as the Wadden Sea interior.

[50] *Schäffer et al.* [1993] show that in phase-resolving Boussinesq wave models the breaking criterion can be related to the slope of the forward face of a shoaling wave. In their approach, waves are assumed to become unstable and break due to the increasing local steepness of the wavefront, and not directly due to the decreasing depth. Such steep forward face slopes are the result of three-wave nonlinear interaction in shallow water, which transforms the wave profile to a sawtooth shape (characterized by nonzero asymmetry of the crests with respect to the vertical) preceding surf breaking [e.g., *Elgar and Guza*, 1986]. This suggests a correlation

between the shallow water nonlinearity of waves, expressed in terms of their evolving asymmetry, and their breaking probability.

[51] Figure 11a shows the relationship between the wave-field asymmetry, computed by

$$A_s = \frac{\langle H(\eta(t))^3 \rangle}{\langle \eta(t)^2 \rangle^{3/2}} \quad (19)$$

and the observed fraction of breaking waves Q_b throughout the surf zone, as recorded by *Boers* [1996], and contained in the present calibration set. In (19), the operator $H(\cdot)$ is the Hilbert transform and $\eta(t)$ is the time series of the surface elevation. It can be seen in Figure 11a that a general

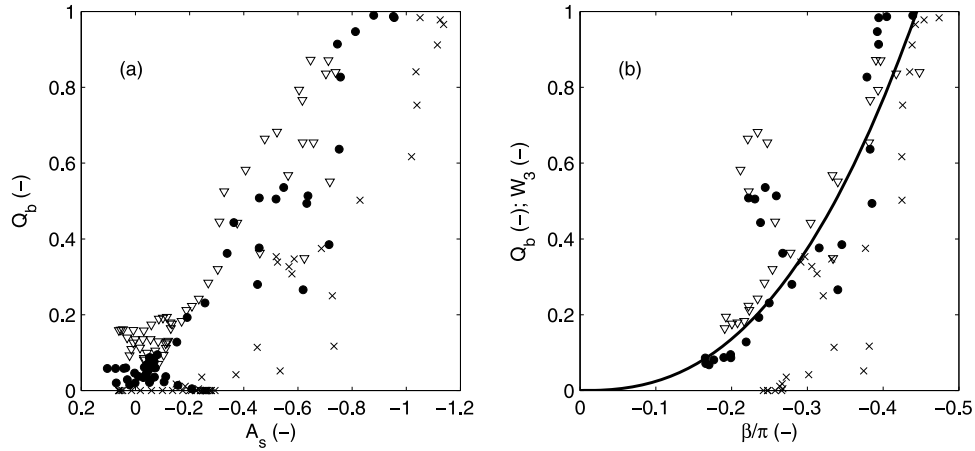


Figure 11. Scatterplots of breaking statistics versus parameters for the wavefield nonlinearity. (a) Q_b versus asymmetry A_s . (b) Q_b versus the biphas β . Solid line indicates the parameterization (22) with $\beta_{\text{ref}} = -4\pi/9$ and $n = 2.5$. Data shown are the cases 1A (solid circles), 1B (inverted triangles), and 1C (crosses) of Boers [1996].

correlation between the asymmetry A_s and Q_b appears to exist throughout the surf zone, low asymmetry corresponds to a low fraction of breakers, whereas high asymmetry corresponds to a high Q_b , and therefore intensive breaking. Boers [1996] also notes this correlation in his data. The data furthermore shows a dependency on the wave steepness. For the case with the lowest wave steepness (case 1C of Boers [1996]), a given Q_b corresponds to the highest wave asymmetry value of the three cases.

[52] The evolution of the wavefield asymmetry A_s is, however, not computed in phase-averaged wave models based only on the energy or action balance equation, such as SWAN. Another variable related to the waveshape is the biphas, the phase angle of the complex bispectrum. Elgar and Guza [1986] show that in a shoaling wavefield on a beach, the observed biphas between the spectral peak frequency and its harmonics evolves from 0 to $-\pi/2$, leading, through three-wave interaction, to the evolution of the wave profile from a vertically symmetrical Stokes wave to a sawtooth shape. As such, the biphas appears to be a suitable variable by which to approximate the asymmetry of the wave profile. However, like the asymmetry, the bispectrum is not computed in operational wave prediction models, so that a parameterization is required. Doering and Bowen [1995] and Eldeberky [1996] have proposed parameterizations for $\beta(f_p, f_p)$, the biphas of the self-interactions of the primary (spectral peak frequency), in terms of the local Ursell number. Here the parameterization of Eldeberky [1996] is used, which reads

$$\beta(f_p, f_p) = -\frac{\pi}{2} + \frac{\pi}{2} \tanh\left(\frac{0.2}{Ur}\right), \quad (20)$$

in which Ur is the Ursell number. The latter is defined as the ratio of the wave steepness ak to the cube of the relative depth, $(kd)^3$. Eldeberky [1996] gives the following spectral mean expression for the Ursell number:

$$Ur = \frac{g}{8\sqrt{2}\pi^2} \frac{H_{m0} T_{m01}^2}{d^2}. \quad (21)$$

[53] Based on the description above, breaking probability in the surf zone can be expected to be related to the biphas $\beta(f_p, f_p)$ (henceforth referred to as β for brevity). For $\beta = 0$, the waves are vertically symmetrical and hence should not break due to bottom influence (although they may still experience steepness-induced breaking). As $\beta \rightarrow -\pi/2$, waves become sawtoothed and break due to an unstable front face, ultimately caused, via three-wave interaction, by the decreasing depth. Figure 11b shows, by means of a scatterplot of Q_b versus β of the Boers [1996] data, that this is indeed the case. Note, however, that $Q_b \approx 1$ is reached somewhere before $\beta = -\pi/2$, namely at a biphas β of around $-4\pi/9$ (or -80°). For values in between these limits, there appears to be a power law relationship between β and Q_b . An exception is found at $\beta \approx -\pi/4$, where an excursion from the power law trend is seen. In space, this corresponds to the region immediately inshore of the bar (compare Figure 6b). Within this region, the magnitude of the biphas β computed using (20) and (21) is likely to be inaccurate, since it depends on local variables only, neglecting its evolution history in space. Due to the strong increase in water depth behind the bar, the magnitude of β drops here, leading to the observed excursion. However, since the bulk of breaking dissipation typically occurs on the seaward face of bars, the model will be shown to perform satisfactorily nonetheless. Hence, it can be concluded that the observations support there being a relationship between β and the fraction of breaking waves of the general form

$$W_3 = Q_b = \left(\frac{\beta}{\beta_{\text{ref}}}\right)^n, \quad (22)$$

in which W_3 represents the fraction of breakers, which has the same form as (11), with n a calibration parameter. The denominator β_{ref} represents the biphas at which all waves are considered to be breaking ($Q_b = 1$), where $W_3 = 1$, and is the second calibration parameter.

[54] The biphas-based expression (22) can replace the γ_{TG} -based expression (11) in the TG83 model as the scaling function of the probability density function of all wave heights (9) to determine the distribution of breaking waves

with (10). In this way, it is assumed that the waves breaking due to their shallow water nonlinearity are distributed proportionally over the probability density function of wave heights. The total dissipation due to depth-induced breaking follows from (8). Since (22) is independent of the individual wave heights H , it can be taken outside of the integral in (8). Integrating, this yields

$$D_{tot} = -\frac{3\sqrt{\pi}}{16} \frac{B^3 \bar{f}}{d} \left(\frac{\beta}{\beta_{ref}} \right)^n H_{rms}^3. \quad (23)$$

[55] The source term follows from substituting (23) in (7). Hereafter, expression (23) is referred to as the biphaser breaker model. It contains a total of three calibration parameters, namely the proportionality coefficient B , the reference biphaser β_{ref} and the exponent n . The calibration of these parameters is considered in section 5.2.

[56] From the model description above, it can be seen that a basic dependency of breaking dissipation on shallow water nonlinearity is proposed, similar to what was suggested by *Massel and Gourlay* [2000]. However, the present expression is defined in terms of the local wave nonlinearity, so as to be applicable to arbitrary evolution of the wavefield, including finite depth wave growth. It should be noted that since the breaker index description pursued here does not feature any explicit maximum wave height at a given depth (as $\gamma_{BJ} = H_m/d$ prescribes), the approach proposed above is not compatible with the details of the BJ78 model in its present form. Two further remarks are made about the proposed breaker scaling: first, based on field observations, TG83 recommend the use of the skewed weighting function (12). This complexity was not included in the present model. Furthermore, Figure 11b shows that the wave condition 1C, with lower steepness than the other two conditions (compare Table 2), reaches higher values of β before breaking. *Doering and Bowen* [1995] note a similar phenomenon for their data set. However, this refinement was not considered in the present model either.

5.2. Calibration and Validation

[57] The biphaser breaker model (23) presented above contains three calibration parameters, namely B , β_{ref} and n . The reference biphaser β_{ref} (where $Q_b = 1$) and the exponent n were fitted to the data of *Boers* [1996]. From the observed relationship between β and Q_b , these parameters were set to $\beta_{ref} = -4\pi/9$ and $n = 2.5$. The resulting fit is shown in Figure 11b. Subsequently, the coefficient B was calibrated using the total calibration subset (Table 3). Figure 12 shows the results of this procedure, in which the value of B was varied over the range 0.5 to 1.5. It can be seen that the sloping bed surf zone cases of Duck and *Boers* [1996] display a strong preference for $B = 0.8$ to 1.0, with a minimum error at $B = 0.90$ (Figure 12c). For the finite depth wave growth cases, by contrast, the results are rather insensitive to the choice of B (Figure 12b). This is because the value of the biphaser is relatively small in these cases, resulting in low levels of dissipation. Hence, the depth-induced breaking term becomes small in the overall action balance, rendering the model results insensitive to the value of B . This result is significant, since it implies that the ratio β/β_{ref} sufficiently

discriminates between sloping bed situations (for which the wavefield is strongly nonlinear) and finite depth growth cases (for which nonlinearity is low), so that no additional parameterizations of the breaker index are required, unlike for γ_{BJ} defined according to (5). Figure 12a shows that the parameter value $B = 0.90$ therefore also suffices for the total calibration set.

[58] The biphaser breaker model (23) with the calibration settings $B = 0.90$, $\beta_{ref} = -4\pi/9$ and $n = 2.5$ is subsequently applied to the validation subset (Table 3). Figure 13 shows an example of the results found for the sloping bed surf zone cases of BJ78, featuring mildly (Run 13 of BJ78, Figure 13a) and violently breaking (Run 15, Figure 13b) cases over a barred beach. It can be seen that the breaker formulation is able to predict both of these distinct breaker conditions well, with nearly the same skill as the BJ78 model.

[59] The progress made with (23) is, however, the ability to also describe the far smaller role played by depth-induced breaking in finite depth wave growth situations. This is shown in Figure 14, which presents a scatterplot comparison between model results and observations for the BJ78 model with a constant $\gamma_{BJ} = 0.73$, and the biphaser breaker model (23). It can be seen that the calibrated expression (23) yields a significant improvement in overall accuracy over the BJ78 model applied with a constant γ_{BJ} : the underprediction of H_{m0} and H_{m0}/d in the Ameland Zeegat and Lake IJssel cases is eliminated, and likewise the overprediction of these variables for the sloping bed surf zone cases of Duck is corrected. The results of the mean wave period $T_{m-1,0}$ are also improved with (23), particularly for the Ameland Zeegat and Duck cases. However, the mean period $T_{m-1,0}$ remains underpredicted in the Lake IJssel cases and, to some extent, in the Ameland Zeegat. As discussed in section 3, this inaccuracy is related to the prediction of the spectral shape, and was not further pursued here. It is interesting to note that the biphaser-scaled expression (23) yields similar improvements to the results found with the breaker index parameterization of *Ruessink et al.* [2003] in Figure 10. Accordingly, the improvement in the overall statistical scores over those of the BJ78 model is comparable to that found with the *Ruessink et al.* [2003] parameterization.

6. Discussion

[60] In this study we have shown that existing bore-based models for depth-induced breaking (e.g., BJ78 and TG83), which have been developed for sloping bed situations, typically yield underpredictions of significant wave height and mean period when applied, with the same breaker index γ , to situations of finite depth wave growth (see, e.g., Figure 10). It was verified that some existing parameterizations of the breaker index γ on additional wavefield parameters yield the required dynamics in dissipation levels to achieve improvement in the overall model performance. In particular, the parameterization of *Ruessink et al.* [2003], who propose a linear dependency of γ_{BJ} on the dimensionless depth $k_p d$, yields a significant improvement in the results of the finite depth growth cases, without negatively affecting those of the sloping bed cases. However, this parameterization remains an adjustment, of which the physical basis is unclear, to the basic variable γ_{BJ} . In addition, since the peak

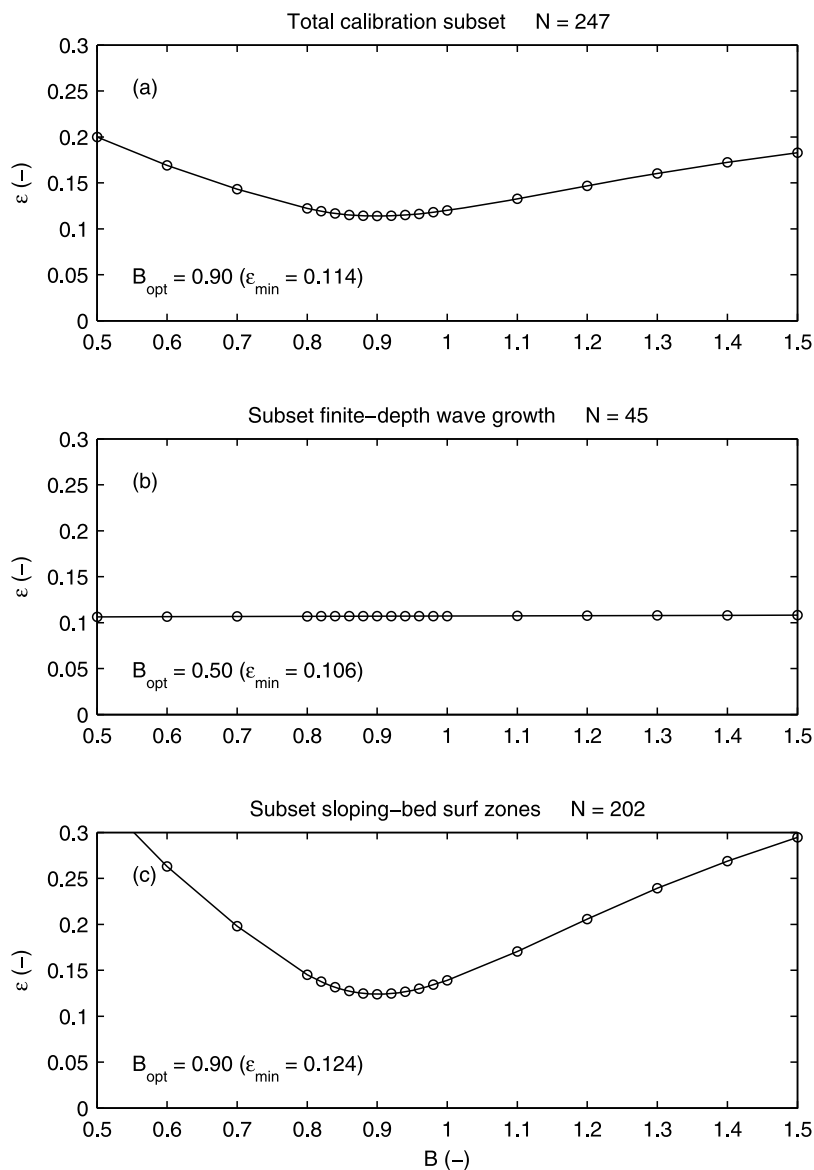


Figure 12. Variation of the error function ε with the coefficient B in the expression (23), for the calibration subset. Shown are (a) the total calibration subset, (b) finite depth wave growth cases, and (c) sloping bed surf zone cases. N indicates the total number of data points included in the statistics.

wave number k_p tends to vary erratically when modeling multimodal spectra, this parameterization is expected to perform well only for unimodal spectra (such as considered in this study).

[61] The nonlinearity-based breaker index (22) proposed in this study, combined with the TG83 model, proved to yield similar generic improvements to the model behavior as the parameterization of *Ruessink et al.* [2003]. However, in addition, the resulting biphase breaker model offers an explanation for the behavior of the BJ78 model combined with this $k_p d$ -dependent breaker index. With the parameterization of *Ruessink et al.* [2003], the lower values of $k_p d$ typically found in sloping bed surf zones yield low values for the breaker index γ_{BJ} , resulting in strong dissipation in the BJ78 model. Conversely, the higher values of $k_p d$ typical of finite depth wave growth situations yield high values of γ_{BJ} , resulting in the required weak dissipation. This model

behavior can be understood physically when viewed in terms of the shallow water nonlinearity of the wavefield, as incorporated in the biphase breaker model: the lower values of $k_p d$ found in sloping bed surf zone situations correspond to higher nonlinearity (through greater values of $Ur = (ak)/(kd)^3$), leading to higher values of β/β_{ref} , steeper forward face slopes, and hence stronger dissipation; conversely, higher values of $k_p d$ signify weaker nonlinearity, yielding lower values of β/β_{ref} , milder forward face slopes and weaker breaking dissipation. These dependencies can be considered analogous to those presented by *Gourlay* [1994] and *Massel and Gourlay* [2000] for the situation of waves breaking on reef fronts.

[62] The proposed biphase breaker model also offers an explanation for the positive relationship between the offshore wave steepness and the breaker index γ_{BJ} found by *Battjes and Stive* [1985] for the BJ78 model, which, as noted by these

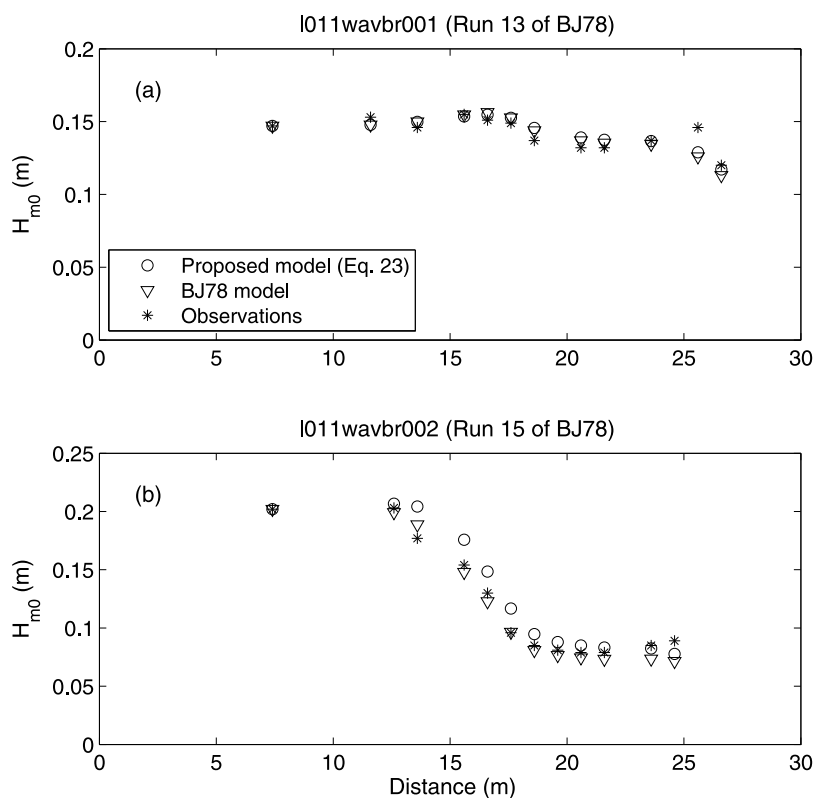


Figure 13. Comparison between the modeled and observed H_{m0} along the flume in the BJ78 experiment, for the proposed model (23) (with $B = 0.90$, $\beta_{\text{ref}} = -4\pi/9$, and $n = 2.5$) and the BJ78 model (with $\gamma_{\text{BJ}} = 0.73$). (a) Run 13 of BJ78, featuring mildly breaking waves. (b) Run 15 of BJ78, featuring violently breaking waves.

authors, is contrary to observations in the laboratory and the field. Examination of their Table 2.1 reveals that the investigated conditions with the lowest and highest, respectively, wave steepness featured approximately the same wave height, but strongly differing wave frequencies: for the higher-frequency case (higher steepness), the optimal γ_{BJ} was found to be high (see also (17)), yielding a low level of dissipation in BJ78. On the other hand, the lower-frequency case (low steepness) yielded a low optimal γ_{BJ} , and hence strong dissipation. Interpreting these results in terms of the shallow water nonlinearity, the following is found: for a similar (offshore) wave height, and at a given depth d , the higher-frequency (higher steepness) case develops smaller Ursell numbers inshore (due to larger k values), leading to a smaller β/β_{ref} and therefore weaker breaking dissipation in the model; conversely, the lower-frequency case (low steepness) develops relatively larger Ursell numbers (due to smaller k values), resulting in a larger β/β_{ref} and hence the greater breaking dissipation observed by *Battjes and Stive* [1985]. Therefore, it appears that by considering the shallow water wavefield nonlinearity, and not just the wave steepness or $k_p d$ individually, a physical basis for the results of *Battjes and Stive* [1985] and *Ruessink et al.* [2003] has been found.

7. Conclusions

[63] The present study aimed to improve the performance of SWAN in situations of finite depth wave growth, particularly over the near-horizontal interior of the Dutch Wadden

Sea. This was achieved first by investigating the optimal settings of the breaker index γ_{BJ} in the BJ78 model, for both sloping bed surf zones and finite depth wave growth situations. Second, from these results, suitable parameterizations for γ_{BJ} from the literature were identified and verified. Third, based on these insights, and earlier work by *Gourlay* [1994] and *Massel and Gourlay* [2000], a new estimation of the breaker index, based on the nonlinearity of the wavefield, is proposed. This breaker index was combined with the model of TG83. The resulting formulation, the biphaser breaker model, was calibrated and validated. From the results of this study, the following can be concluded:

[64] 1. The behavior of the model error as a function of γ_{BJ} (taken as spatially constant) produced with the BJ78 model differs significantly between cases representing sloping bed surf zones on the one hand, and finite depth wave growth conditions on the other. For surf zones, clear optimal values of γ_{BJ} are found in the investigated parameter range. By contrast, under finite depth wave growth conditions, model errors asymptotically decrease with increasing values of γ_{BJ} . This result suggests that the process of depth-induced breaking should play a minimal role in the model under such conditions. This result is supported by field observations by *Babanin et al.* [2001].

[65] 2. The above conclusion suggests that no single, constant value of the breaker index γ_{BJ} can be found that would significantly improve on the general performance of the BJ78 dissipation term with a constant $\gamma_{\text{BJ}} = 0.73$ for both sloping bed and finite depth wave growth situations.

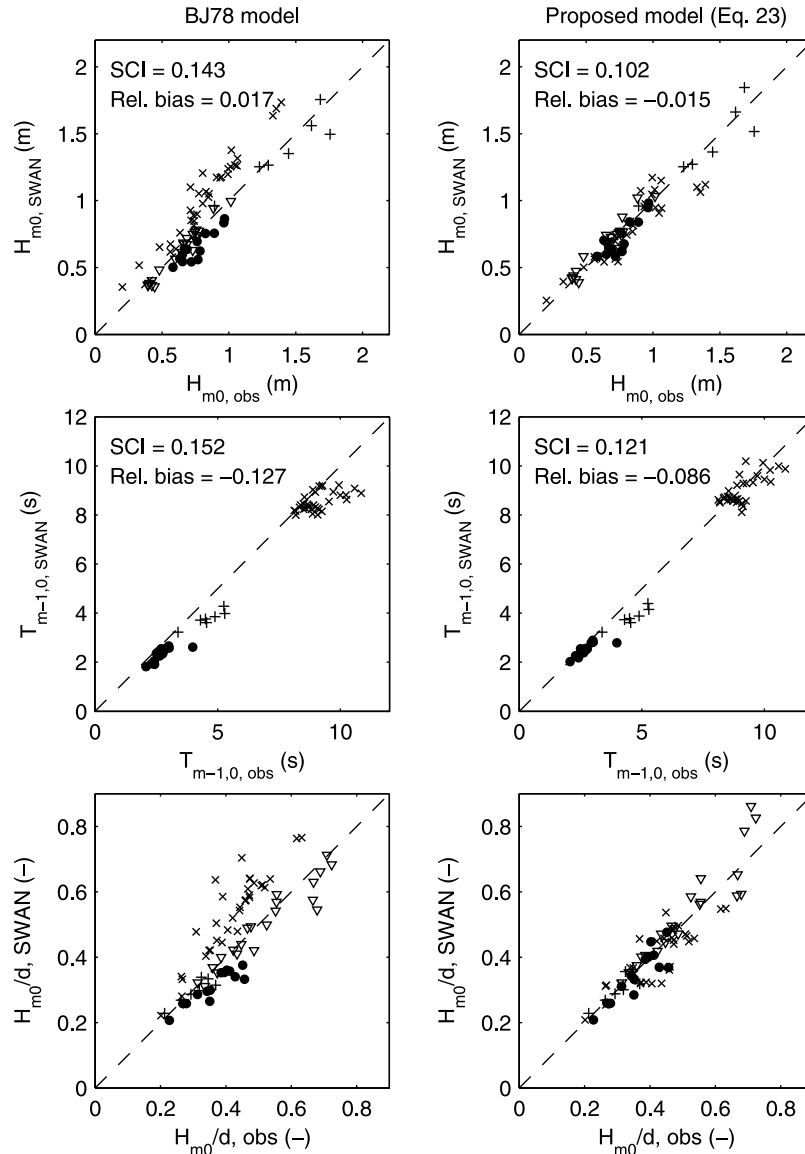


Figure 14. Scatterplots of model results versus observations of the validation subset for (left) the BJ78 model (with $\gamma_{BJ} = 0.73$) and with (right) the proposed model (23) (with $B = 0.90$, $\beta_{ref} = -4\pi/9$ and $n = 2.5$). Plotted are results of Amelanders Zeegat (solid circles), Lake IJssel (pluses), Duck (crosses), and the BJ78 flume (inverted triangles). Wave height data of BJ78 are scaled up by a factor of 5 for presentation purposes.

[66] 3. In both the sloping bed surf zone and finite depth wave growth situations, optimal values of γ_{BJ} correlate with the dimensionless depth $k_p d$ for cases with approximately $k_p d < 1$. Hence, it was found that the parameterization of γ_{BJ} as a function of $k_p d$, derived by *Ruessink et al.* [2003] for sloping bed surf zone situations, is also applicable to finite depth wave growth situations. However, due to its definition in terms of the peak wave number k_p , this parameterization is only considered suitable for modeling unimodal spectra in its present form.

[67] 4. Analysis of observed fractions of breakers suggests that, analogous to techniques applied in phase-resolving wave models, the breaking process in phase-averaged wave models can be related to the evolution of the forward face slope of the waves through a dependency on the wave asymmetry. Equivalently, this can be embodied in a dependency

of wave breaking on the biphasic of the self-interactions of the spectral peak. The latter can be approximated in operational phase-averaged wave models by means of published empirical dependencies on the local Ursell number.

[68] 5. The nonlinearity-based breaker index proposed in this study, in combination with the TG83 model, has been shown to yield a significant improvement in overall accuracy compared to that of the BJ78 model using a constant $\gamma_{BJ} = 0.73$, particularly for situations of finite depth wave growth. For these situations, the proposed biphasic breaker model succeeds in predicting the much lower degree of depth-induced dissipation required in the model, and reported in the field under similar conditions. These improvements in accuracy are of the same order as those found with the γ parameterization of *Ruessink et al.* [2003] applied to the BJ78 model.

[69] 6. Unlike the breaker index parameterization of Ruessink et al. [2003], the proposed biphasic breaker model provides a physical explanation, in terms of differing degrees of nonlinearity, for the observed model behavior with respect to depth-induced breaking.

[70] **Acknowledgments.** The presented work is part of the SBW (Strength and Loads on Water Defenses) project commissioned by Rijkswaterstaat Centre for Water Management in the Netherlands. The author would also like to thank Jurjen Battjes and Leo Holthuijsen for their helpful comments on this work.

References

- Aptosos, A., B. Raubenheimer, S. Elgar, and R. T. Guza (2008), Testing and calibrating parametric wave transformation models on natural beaches, *Coastal Eng.*, *55*, 224–235.
- Babanin, A. V., I. R. Young, and M. L. Banner (2001), Breaking probabilities for dominant surface waves on water of finite constant depth, *J. Geophys. Res.*, *106*(C6), 11,659–11,676.
- Baldock, T. E., P. Holmes, S. Bunker, and P. van Weert (1998), Cross-shore hydrodynamics within an unsaturated surf zone, *Coastal Eng.*, *34*, 173–196.
- Battjes, J. A., and S. Beji (1992), Breaking waves propagating over a shoal, in *Coastal Engineering, 1992*, edited by B. L. Edge, pp. 42–50, Am. Soc. of Civ. Eng., New York.
- Battjes, J. A., and J. P. F. M. Janssen (1978), Energy loss and set-up due to breaking of random waves, in *Coastal Engineering, 1978*, pp. 569–588, Am. Soc. of Civ. Eng., New York.
- Battjes, J. A., and M. J. F. Stive (1985), Calibration and verification of a dissipation model for random breaking waves, *J. Geophys. Res.*, *90*(C5), 9159–9167.
- Birkemeier, W. A., C. Donoghue, C. E. Long, K. K. Hathaway, and C. F. Baron (1997), The 1990 DELILAH nearshore experiment: Summary report, *Tech. Rep. CHL-97-24*, 217 pp., U.S. Army Corps of Eng., Vicksburg, Miss.
- Boers, M. (1996), Simulation of a surf zone with a barred beach, report 1: Wave heights and wave breaking, *Commun. Hydr. Geotech. Eng.*, *96-5*, 116 pp.
- Booij, N., R. C. Ris, and L. H. Holthuijsen (1999), A third generation wave model for coastal regions: 1. Model description and validation, *J. Geophys. Res.*, *104*(C4), 7649–7666.
- Bottema, M., and D. Beyer (2002), Evaluation of the SWAN wave model for the Dutch IJsselmeer area, in *Ocean Wave Measurement and Analysis*, edited by B. L. Edge and J. Michael Hemsley, pp. 560–569, Am. Soc. of Civ. Eng., Reston, Va.
- Bottema, M., and G. P. van Vledder (2009), A ten-year data set for fetch- and depth-limited wave growth, *Coastal Eng.*, *56*, 703–725, doi:10.1016/j.coastaleng.2009.01.012.
- Bottema, M., J. P. de Waal, and H. J. Regeling (2003), Some applications of the Lake IJssel/Lake Sloten wave data set, in *Coastal Engineering 2002*, edited by J. McKee Smith, pp. 413–425, Am. Soc. of Civ. Eng., New York.
- Bretschneider, C. L. (1958), Revised wave forecasting relationships, paper presented at 6th Conference on Coastal Engineering, Am. Soc. of Civ. Eng., Gainesville, Fla.
- De Waal, J. P. (2002), Wave growth limit in shallow water, in *Ocean Wave Measurement and Analysis*, edited by B. L. Edge and J. Michael Hemsley, pp. 580–589, Am. Soc. of Civ. Eng., Reston, Va.
- Doering, J. C., and A. J. Bowen (1995), Parameterization of orbital velocity asymmetries of shoaling and breaking waves using bispectral analysis, *Coastal Eng.*, *26*, 15–33.
- Donelan, M. A., A. V. Babanin, I. R. Young, and M. L. Banner (2006), Wave-follower field measurements of the wind-input spectral function, part II: Parameterization of the wind input, *J. Phys. Oceanogr.*, *36*, 1672–1689.
- Eldeberky, Y. (1996), Nonlinear transformations of wave spectra in the nearshore zone, Ph.D. thesis, 203 pp., Delft Univ. of Technol., Delft, Netherlands.
- Eldeberky, Y., and J. A. Battjes (1996), Spectral modeling of wave breaking: Application to Boussinesq equations, *J. Geophys. Res.*, *101*, 1253–1264.
- Elgar, S., and R. T. Guza (1986), Nonlinear model predictions of bispectra of shoaling surface gravity waves, *J. Fluid Mech.*, *167*, 1–18.
- Gourlay, M. R. (1994), Wave transformation on a coral reef, *Coastal Eng.*, *23*, 17–42.
- Groeneweg, J., A. J. van der Westhuisen, G. P. van Vledder, S. Jacobse, J. Lanser, and A. R. van Dongeren (2008), Wave modeling in a tidal inlet: Performance of SWAN in the Wadden Sea, in *Coastal Engineering 2008*, edited by J. McKee Smith, pp. 411–423, Am. Soc. of Civ. Eng., New York.
- Hasselmann, K., et al. (1973), Measurement of windwave growth and swell decay during the Joint North Sea Wave Project (JONSWAP), *Dtsch. Hydrogr. Z.*, *A8*(12), 95 pp.
- Hasselmann, S., K. Hasselmann, J. A. Allender, and T. P. Barnett (1985), Computations and parameterizations of the nonlinear energy transfer in a gravity-wave spectrum. Part 2: Parameterization of the nonlinear transfer for application in wave models, *J. Phys. Oceanogr.*, *15*, 1378–1391.
- Holthuijsen, L. H., and N. Booij (2006), Experimental wave breaking in SWAN, in *Coastal Engineering 2006*, edited by J. McKee Smith, pp. 392–402, Am. Soc. of Civ. Eng., New York.
- Holthuijsen, L. H., M. Zijlema, and P. J. van der Ham (2008), Wave physics in a tidal inlet, in *Coastal Engineering 2008*, edited by J. McKee Smith, pp. 437–448, Am. Soc. of Civ. Eng., New York.
- Komen, G. J., S. Hasselmann, and K. Hasselmann (1984), On the existence of a fully developed wind-sea spectrum, *J. Phys. Oceanogr.*, *14*, 1271–1285.
- Massel, S. R., and M. R. Gourlay (2000), On the modeling of wave breaking and set-up on coral reefs, *Coastal Eng.*, *39*, 1–27.
- Nairn, R. B. (1990), Prediction of cross-shore sediment transport and beach profile evolution, Ph.D. thesis, 391 pp., Imperial Coll., London.
- Nelson, R. C. (1985), Wave heights in depth limited conditions, *Trans. Inst. Eng. Aust.*, *27*, 210–215.
- Nelson, R. C. (1994), Depth limited design wave heights in very flat regions, *Coastal Eng.*, *23*, 43–59.
- Ruessink, B. G., D. J. R. Walstra, and H. N. Southgate (2003), Calibration and verification of a parametric wave model on barred beaches, *Coastal Eng.*, *48*, 139–149.
- Schäffer, H. A., P. A. Madsen, and R. Deigaard (1993), A Boussinesq model for waves breaking in shallow water, *Coastal Eng.*, *20*, 185–202.
- Snyder, R. L., F. W. Dobson, J. A. Elliot, and R. B. Long (1981), Array measurements of atmospheric pressure fluctuations above surface gravity waves, *J. Fluid Mech.*, *102*, 1–59.
- Swart, D. H., and C. C. Laubser (1978), Vocoidal theory for full non-breaking waves, in *Coastal Engineering, 1978*, pp. 467–486, Am. Soc. of Civ. Eng., New York.
- Thornton, E. B., and R. T. Guza (1983), Transformation of wave height distribution, *J. Geophys. Res.*, *88*, 5925–5938.
- van der Westhuisen, A. J., and G. P. van Vledder (2008), Speeding up stationary SWAN computations by dynamic grid point deactivation, paper presented at 31th International Conference Coastal Engineering, Am. Soc. of Civ. Eng., Hamburg, Germany.
- van der Westhuisen, A. J., M. Zijlema, and J. A. Battjes (2007), Nonlinear saturation-based whitecapping dissipation in SWAN for deep and shallow water, *Coastal Eng.*, *54*, 151–170.
- van Vledder, G. P., J. Groeneweg, and A. J. van der Westhuisen (2008), Numerical and physical aspects of wave modeling in a tidal inlet, paper presented at 31th International Conference Coastal Engineering, Am. Soc. of Civ. Eng., Hamburg, Germany.
- Vink, A. S. (2001), Transformation of wave spectra across the surf zone, M.Sc. thesis, 72 pp., Delft Univ. of Technol., Delft, Netherlands.
- Young, I. R., and A. V. Babanin (2006), The form of the asymptotic depth-limited wind wave frequency spectrum, *J. Geophys. Res.*, *111*, C06031, doi:10.1029/2005JC003398.
- Young, I. R., and L. A. Verhagen (1996), The growth of fetch-limited waves in water of finite depth. Part 1. Total energy and peak frequency, *Coastal Eng.*, *29*, 47–78.
- Zijderfeld, A., and H. Peters (2008), Measurement programme Dutch Wadden Sea, paper presented at 31th International Conference Coastal Engineering, Am. Soc. of Civ. Eng., Hamburg, Germany.
- Zijlema, M., and A. J. van der Westhuisen (2005), On convergence behaviour and numerical accuracy in stationary SWAN simulations of near-shore wind wave spectra, *Coastal Eng.*, *52*, 237–256.

A. J. van der Westhuisen, Hydraulic Engineering Unit, Delft Hydraulics, Deltares, Rotterdamseweg 185, NL-2629 HD Delft, Netherlands. (andre.vanderwesthuisen@deltares.nl)